THESIS
2
2007

This is to certify that the
thesis entitled

Low Resistance Contacts to Thermoelectric Materials

presented by

Jonathan James D'Angelo

has been accepted towards fulfillment
of the requirements for the

M.S. degree in Electrical and Computer Science Engineering

Major Professor's Signature

May 1, 2006

Date

MSU is an Affirmative Action/Equal Opportunity Institution

LIBRARY
Michigan State
University

PLACE IN RETURN BOX to remove this checkout from your record.
TO AVOID FINES return on or before date due.
MAY BE RECALLED with earlier due date if requested.

DATE DUE	DATE DUE	DATE DUE

2/05 p:/CIRC/DateDue.indd-p.1

LOW RESISTANCE CONTACTS TO THERMOELECTRIC MATERIALS

By

Jonathan James D'Angelo

A THESIS

Submitted to
Michigan State University
In partial fulfillment of the requirements
for the degree of

MASTER OF SCIENCE

Department of Electrical and Computer Engineering

2006

ABSTRACT

LOW RESISTANCE CONTACTS TO THERMOELECTRIC MATERIALS

By

Jonathan James D'Angelo

Thermoelectric generators operate with no moving parts to convert heat flow to electricity. Low electrical contact resistance is essential for the fabrication of high efficiency thermoelectric generators. These contacts must be stable to high temperatures and through thermal cycling. Here we present the fabrication procedure and characterization of several contacts to Pb-Sb-Ag-Te (LAST) and Pb-Sb-Ag-Sn-Te (LASTT) compounds. Several measurement systems have been developed for characterization of the materials and contact resistances. A diffusion bonding system has also been developed and utilized for investigating various metal contacts. Contact resistances less than $50\mu\Omega\cdot cm^2$ have been achieved for several diffusion bonded metals, and solder junctions. In addition, sputtering and e-beam deposition of various metal contacts were investigated. The development of these systems, and the results obtained is presented along with the processes for fabricating an entire thermoelectric power generation module.

Table of Contents

LIST OF TABLES

LIST OF FIGURES

Chapter 1 Overview

1.1 The "Thermomagnetic Effect"

In early 1820, a young scientist by the name of Thomas Seebeck was experimenting with the possibility of a relationship between heat and electricity [1]. His experimental setup was a current loop formed by the junctions at both ends of a copper and a bismuth wire. Seebeck heated up one of the copper-bismuth junctions while the other remained at room temperature. What he measured was a magnetic field radiating from the wire. He believed that the temperature gradient was causing the magnetic field. He called this the "Thermomagnetic Effect." This is was wrong. The magnetic field that he measured was produce by the current flowing due to the temperature gradient in the current loop, however the relationship between current flow and magnetic field was not known at that time. If one of the wires is cut, then no magnetic field results; instead a voltage can be measured at the open circuit terminals. This voltage is the Seebeck coefficient for the junction formed by those metals, and is a temperature integral sum of the thermopowers (or absolute Seebeck coefficients) of each metal.

In 1834 when another scientist by the name of Peltier discovered that when electricity is forced to flow through a junction of dissimilar metals, heat would either be absorbed or liberated at the junction based on the direction of current flow.[2].

Later Thomson showed that heating or cooling along the length of a single material also takes place when electrical current flows through the material. This became known as the Thomson Effect. Today's thermoelectric devices are based on these scientific principles.

1.2 Advantages of Thermoelectrics

The science of thermoelectrics was born some time ago, but only in recent days has it grown to become available commercially. Most thermoelectrics are used for cooling and heating devices. A thermoelectric cooler can be bought at your local stores. A list of advantages is [3];

1. No moving parts for long device lifetimes and little maintenance
2. They can be made into small or large devices without loss of efficiency
3. The same module can be used as a power generator and a cooler
4. They can operate in any orientation
5. They give very little electronic noise

1.3 Current Research

The goal of the transport characterization laboratory here at Michigan State University is to build a twenty percent efficient, one kilowatt generator. The generator will be operating under a temperature gradient of ~580 degrees (room temperature to 600°C). Common thermoelectric materials and their maximum operating temperatures is given in Table 1 below.

Table 1: Common thermoelectric materials, their maximum operating temperature, maximum efficiency (Z), and the temperature of Zmax.

	Z_{max} (K^{-1})	Useful Range	T_{Zmax} (K)
Bi_2Te_3	$3x10^{-3}$	< 500 K	300
PbTe	$1.7x10^{-3}$	< 900 K	650
Si-Ge	$1x10^{-3}$	< 1300 K	1100

Most bismuth telluride modules operate near room temperature where solder contacts can be used on both the hot and cold side junctions. The devices built here at Michigan State University need to have bonds on the hot side of the device that can withstand rigorous temperature cycling and high temperature operations where solder contacts are not possible.

The Chemistry Department at Michigan State University has discovered several chalcogenide based materials that have shown promising thermoelectric properties [4]. Recently compounds in the $Ag_{1-x}Pb_mSbTe_{2+m}$ and $Ag(Pb_{1-x}Sn_x)_mSbTe_{2+m}$ systems have exhibited outstanding thermoelectric properties for power generation applications [5]. Lead antimony silver tellurium or also know as LAST and lead-antimony-silver-tin-tellurium, or LASTT, are the n-type and p-type materials (respectively) used for fabrication of the thermoelectric devices. The purpose of this thesis is to investigate both high and

low temperature contacts to this material. The contact resistance of a thermoelectric device is a loss to the efficiency of the device (through ohmic heating) and thus should be minimized. As part of this thesis, many materials have been tested and various contact resistance measurement systems were developed.

1.4 Thermoelectric Devices

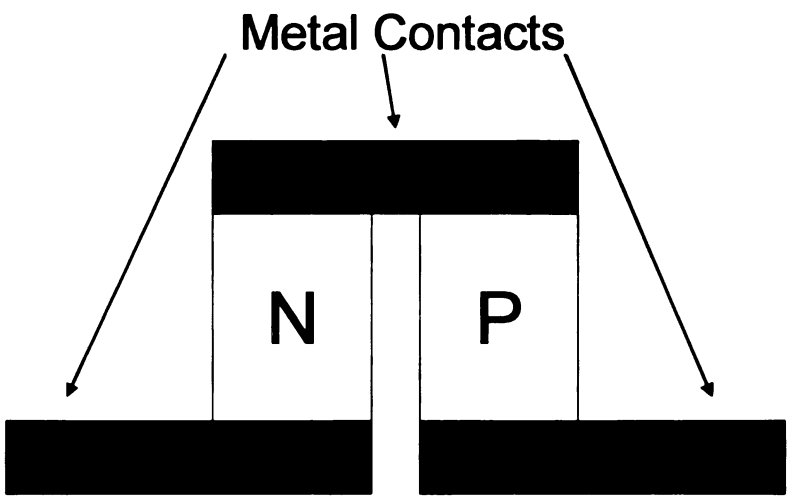

Figure Intro 1: Thermoelectric Device

Figure 1 shows a single junction (unicouple) between n-type and p-type thermoelectric material in a standard thermoelectric device. Both the n-type and p-type materials are doped to degeneracy and form ohmic contacts to the electrodes; thus although it is an n-type to p-type structure it does not form a diode and these devices exhibit linear current vs. voltage profiles.

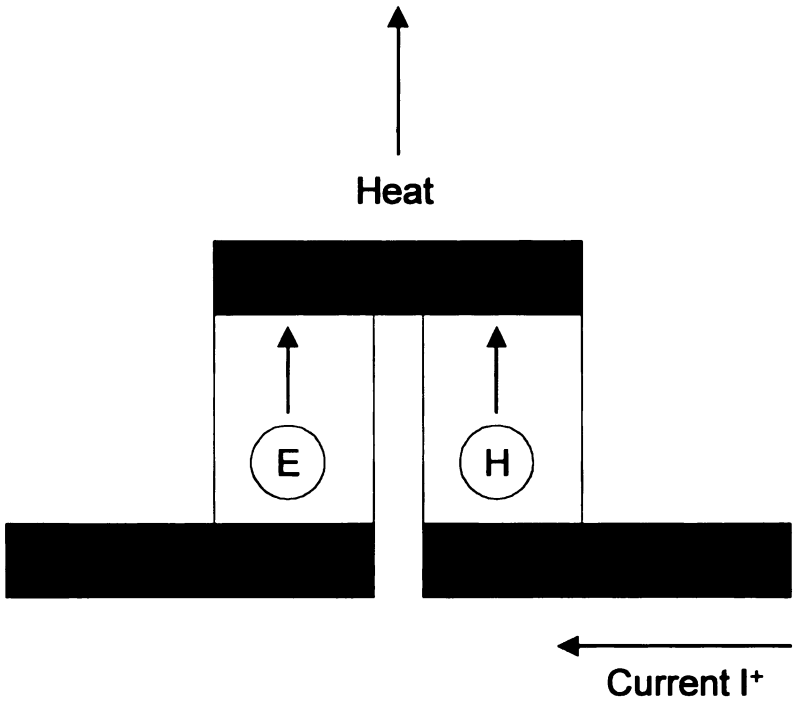

Figure Intro 2: Thermoelectric heating device (E-Electrons in n-type leg, H-Holes in p-type leg)

By supplying electrical power to this device as shown in Figure 2, heat can be pumped from one side of the device to the other to establish a temperature gradient. Heat will flow through the p-type leg in the same direction as the electrical current flow through that leg. The carriers, or holes, in the p-type material move in the direction of current flow and also carry heat from the bottom of the device to the top. The electrons on the n-type side are also moving in the same upwards direction along the device, also carrying heat. This makes the top side of the device hot and cools the bottom of the device as shown in Figure 2. With this same layout and reversing the current direction, the top of the device will then be cooled following the same principles.

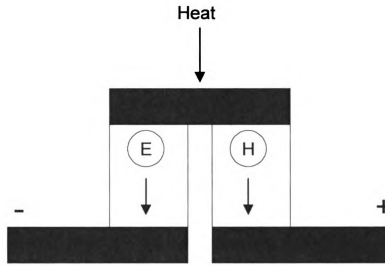

Figure Intro 3: Thermoelectric power generation device

These devices, thus serve as heat pumps. If instead of supplying electrical power to the device in order to create a temperature gradient, a temperature gradient is supplied to the device, then electrical power can be generated. The larger the temperature gradient the more voltage produced by the module. The heat that is supplied by the module is carried to the cold side of the device by the electrons in the n-type and the holes in the p-type. This makes one side a positive potential and the other a negative. This can be attached to an electrical circuit and be used as a power supply. The concept is relatively simple, but these devices do have their limits. There efficiencies are very low (typically ~5% for Bi_2Te_3 based devices).

Chapter 2 Characterizing Thermoelectric Materials

2.1 What Makes a Good Thermoelectric?

Every thermoelectric material is rated by its figure of merit, *ZT*. *ZT* is a dimensionless quantity given by

$$ZT = \frac{S^2\sigma}{\kappa} \cdot T \quad (1)$$

where *S* is the thermopower, σ is the electrical conductivity, κ is thermal conductivity, and *T* is temperature. To obtain a high *ZT* the thermopower and conductivity must be high along with a low thermal conductivity. All of these quantities are temperature dependent. All of three of these quantities are measured here at MSU. Maximizing *ZT* can be challenging as these materials properties are not independent of one another. Usually a material that has a higher electrical conductivity will have a high the thermal conductivity. This behavior is seen in most conductors, such as copper, and insulators, such as glass. Optimization of the three material properties is generally found in heavily doped semiconductors [6].

2.2 Electrical Conductivity

The electrical conductivity has a direct relation to the dopant concentration of a semiconductor material.

$$\sigma = q(\mu_n \cdot n + \mu_p \cdot p) \quad (2)$$

In equation (2), *n* and *p* are the dopant concentrations of a semiconductor material. The concentration of dopants in LAST materials is around 10^{19} cm^{-3}.

At this concentration, the sample is degenerately doped and shows metallic temperature dependence for the electrical conductivity (decreasing σ with increasing temperature). We have experimentally found electrical conductivity values in the range of 800 to1500 $S \cdot cm^{-1}$ to correspond to some of the highest *ZT* samples.

2.3 Thermopower

The thermopower of a device, or also known as the Seebeck coefficient is the open circuit voltage of a semiconductor under the influence of a temperature gradient. The thermopower of a material is a measure of the local entropy, and is influenced by effective masses and the energy dependence of the density of states. For LAST materials we have experimentally found values near $100 \mu V \cdot K^{-1}$ at room temperature tend to yield the highest *ZT* materials. When adjusting the composition and doping of LAST, a reduction in the carrier concentration causes an increase in the thermopower, however also corresponds to a decrease in the electrical conductivity.

$$S = \frac{\pi^2 k^2 T}{3e} \cdot \frac{d \ln \sigma(E)}{dE}\bigg|_{E=E_f} \quad (3)$$

Equation above is the Boltzmann transport theory equation for thermopower, the Mott equation [3]. The electrical conductivity in the equation is a function of the Fermi energy. The thermopower is directly proportional to the derivative of the

density of states. Current research is looking for more complex structures with materials that have 2D, 1D and 0D structures.

2.4 Thermal Conductivity

The thermal conductivity is the measurement of a materials ability to conduct heat. From equation (1) it can be seen that a low thermal conductivity material helps to increase the figure of merit. For the materials studied in this thesis, a thermal conductivity near $1 W \cdot m^{-1} \cdot K^{-1}$ is commonly seen for the high ZT samples. There are two contributions to thermal conductivity.

$$\kappa = \kappa_e + \kappa_l \quad (4)$$

The first part is the electronic contribution and the second part is the lattice (or phonon) contribution to the thermal conductivity. For metals, the electronic contribution to the thermal conductivity was found to obey the Weidemann-Franz law

$$\kappa_e = L \cdot \sigma \cdot T \quad (5)$$

where L is the Lorentz number, σ is the electrical conductivity of the material, and T is the temperature. This indicates that a trade off between high electrical conductivity and low thermal conductivity must be considered for optimizing the ZT of a sample.

The lattice thermal conductivity can also be adjusted through mass fluctuations within the crystal lattice. This can be accomplished through the choice of multielement semiconductor materials containing high and low mass elements, and through alloying of materials. More recently, the prediction of *ZT* enhancements through quantum confinement [7] has led to thin film materials that exhibit high *ZT* values primarily through a significant reduction in thermal conductivity [8]. The LAST and LASTT bulk materials developed at Michigan State University also exhibit endotaxially imbedded nanostructures which form during ingot growth through a spinodal decomposition mechanism [5]. These nanostructures are believed to reduce electron-phonon interaction by preferentially scattering phonons while allowing electrons to flow through them.

2.5 Contact Resistance

Reduction in the contact resistance is crucial for building an efficient thermoelectric device. The contact resistance comes from the interface of to dissimilar metals or a semiconductor to a metal. Also for a good thermoelectric device all electrical contacts must be ohmic. An ideal ohmic contact is a perfect source and sink of both holes and electrons. A nonlinear contact would have diode behaviors. The losses due to I^2R from the contact have to be reduced. Below is the derivation of how the contact resistance directly affects the efficiency of a device.

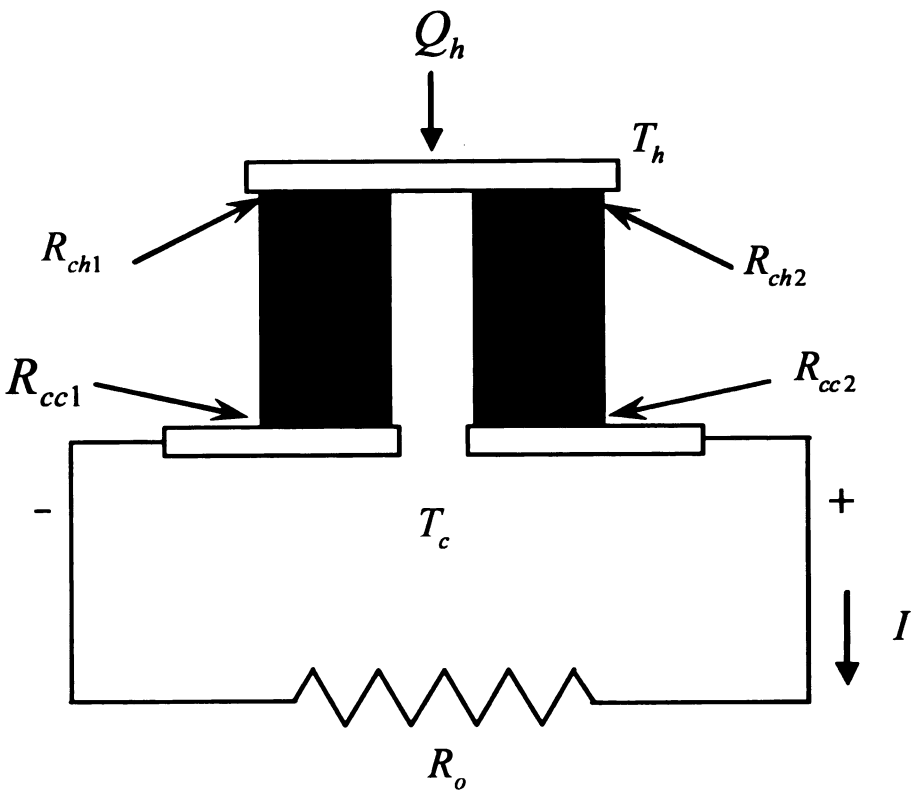

$$\eta = \frac{P_o}{Q_h} \quad (6),$$

$$P_o = I^2 R_o \quad (7),$$

$$Q_h = K\Delta T + ST_h I - \frac{1}{2} I^2 (R + R_c) \quad (8),$$

$$\eta_c = \frac{\Delta T}{T_h} \quad (9),$$

$$\mu = \sqrt{(1+\delta)^2 + (1+\delta) Z T_{av}} \quad (10),$$

$$\delta = \frac{R_c}{R} = \frac{R_{cc1} + R_{cc2} + R_{ch1} + R_{ch2}}{R_n + R_p} \quad (11),$$

$$\eta = \frac{\mu\eta_c}{\frac{(\mu+1+\delta)^2}{ZT_h} + (\mu+1+\delta) - \frac{(1+\delta)\eta_c}{2}} \quad (12).$$

Equation (12) gives the overall efficiency of a device. Figure (Intro.4) below shows plots of the relationship between contact resistance and module efficiency.

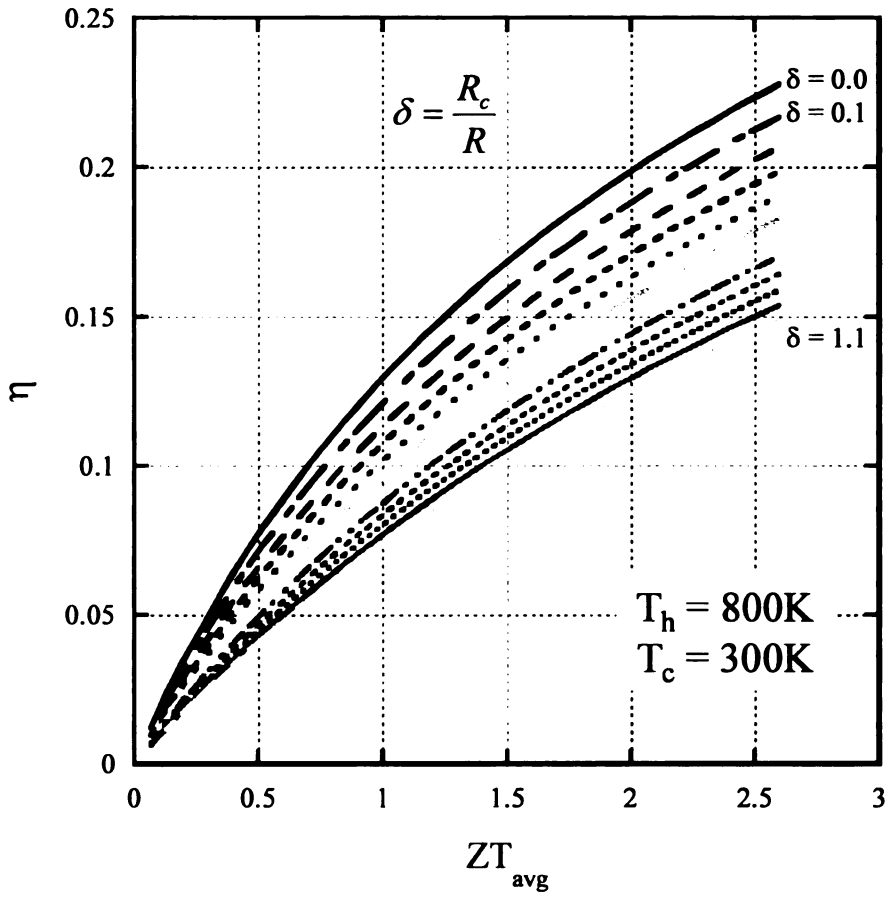

Figure Intro 4: Efficiency degradation due to contact resistance[9]

As is further described in this thesis various contact metals have been investigated for contacts to LAST and LASTT materials. A description of the diffusion bonding system, and the results obtained from it are discussed. In addition, several measurement systems specifically developed for testing the contact resistance have been developed, and are described in this thesis.

Chapter 3 Depositing and Measuring Contacts

3.1 Introduction

Electrical contacts to our thermoelectric devices are needed to ensure an overall promising efficiency. The goal of this thesis is to investigate low resistance contacts to new thermoelectric materials of $Ag_{1-x}Pb_mSbTe_{2+m}$ and $Ag(Pb_{1-x}Sn_x)_mSbTe_{2+m}$. As part of this study, systems were developed to measure contact resistances, and a furnace system was developed for diffusion bonding of various metal contacts to the thermoelectric materials. The materials investigated were all contacts to LAST (lead antimony silver tellurium) and LASTT (LAST with tin) materials. The contact metals to be measured were also deposited to the materials by different methods which are described below.

3.2 Transmission Line Model

The contact resistance of a junction can be obtained by measuring the position dependent voltage profile through the junction. This is a common technique for determining the contact resistance for fabricated devices, however for small contact resistances, the discontinuity in the voltage across the junction can be very small. Under such conditions the transmission line model (TLM) technique [10] is a more accurate measurement of the contact resistance. This technique uses planar contacts to bulk materials to measure contact resistance. By measuring the resistance between these pads, a simple calculation can then be done to obtain the overall contact resistance in units of $\mu\Omega cm^2$.

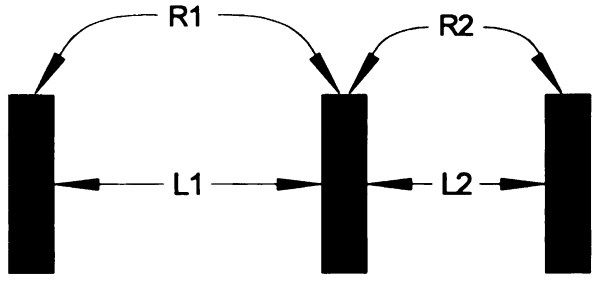

Figure 1: Diagram of planar contacts to a bulk material. L1 and L2 can be any lengths chosen by the user as long as one contact does not interfere electrically with another contact.

Once this setup is achieved, two simple resistance measurements are needed followed by the calculation of the contact resistance.

$$R_c = \frac{R_2 \cdot L_1 - R_1 \cdot L_2}{2(L_1 - L_2)} \qquad (1)$$

This will give you the contact resistance of your contact metal to your bulk material. This calculation can be easily derived for any material. The only assumption this calculation uses is that the material along lengths L_1 and L_2 are uniform in electrical conductivity. If they are not, the ratio of the two resistances will not be correct and then the calculation would yield an improper contact resistance.

The TLM method is more accurate, however the configuration of the contacts for the TLM method is not always amiable to the final device configuration. Therefore, both measurement techniques are valuable in the course of developing thermoelectric generators. Several contact materials have been investigated using the TLM method by depositing the contact materials with sputtering and electron beam evaporation techniques.

3.3 Sputtering

Sputtering is a method of depositing thin films to a substrate by repetitively accelerating ionized atoms of a noble gas (typically argon) into a target material. The energy of these accelerated argon atoms are transferred to the atoms in the target, which expels them from the target surface, and are collected onto the substrate. This technique has been likened to a game of atomic billiards. A noble gas is used as the sputtering atoms since it will not easily be incorporated into the deposited film. The atoms of argon are first ionized in a plasma and then are accelerated by a large electric potential.

There are two main types of sputtering, Direct Current (DC) and Radio Frequency (RF). DC sputtering can only be used for conducting materials, while RF can be used for both conducting and insulating materials. Both methods were used in this investigation.

Sputtering rates and film thickness are dependent on the argon pressure and power used. These yields can be found in most litterateurs, or can be found experimentally. Various sputtering systems check pressures at different locations and may have varying power capabilities, and electrode configurations, therefore sputtering yields can change from system to system.

Sputtering instructions are as follows;

1. Inside chamber loosen the dark space shield retaining screws and slide the dark space shield off the surface.

2. Loosen the 4-target hold down screws and rotate the hold down ring to a position where the through holes are directly beneath the screw heads. The hold down ring can now be taken off.
3. Remove old target and install new one
4. Replace the target hold-down ring over the 4 protruding screws and rotate the ring so that the screw heads are not aligned with the through holes. Tighten down the screws to secure the hold down ring over the target.
5. Replace the dark shield and tighten the dark space shield retaining screws.
6. IMPORTANT! Visually inspect the gap between the dark space shield and the target hold-down ring; it should measure at least 1/16"
7. Pump down system to a vacuum of lower than 20mTorr (vacuum level is user determined)
8. When achieved... close hi-vac and open high wac throttle, and process gas.
9. Set gas pressure by adjusting the gas inlet. Want about 5mTorr of argon.
10. Turn on power supply and adjust the output until plasma is observed.
11. Let target wear in for 5-10 minutes.
12. Sputter to desired film thickness. Rates depend on pressures and power.

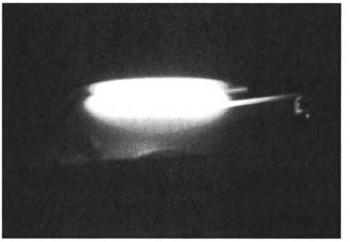

Figure 2: Above is pictured the plasma of the sputtering process

The sputtering plasma is a bright purple glow. After the process is completed, let the system cool for about a half hour, and then shut off the pump and vent the system.

3.4 Electron Beam (E-Beam) Deposition

Electron beam deposition is an evaporation technique for depositing thin films. This is a good deposition technique for many materials, but does not work well for some materials. In the physical vapor deposition (PVD) system located in the Engineering Research Complex Cleanroom, a quartz crystal monitor is used to accurately measure film thickness during deposition. This e-beam system is able to hold up to four different evaporation sources at one time.

An electron beam is guided by a magnetic field and controlled by a set of deflection plates to melt the target material. Once the melted material enters the vapor phase it follows a direct path up through the PVD chamber and deposits

onto a substrate located on a rotating platen. Within this deposition system, sample must be attached to the rotating platen in a way that allows the platen to be flipped upside down during deposition. Because of this, and the size of our substrates, special masks had to be developed for deposition.

3.5 Deposition Masks

The first mask developed for contact resistance research was the Transmission Line Mask shown in Figure 3.

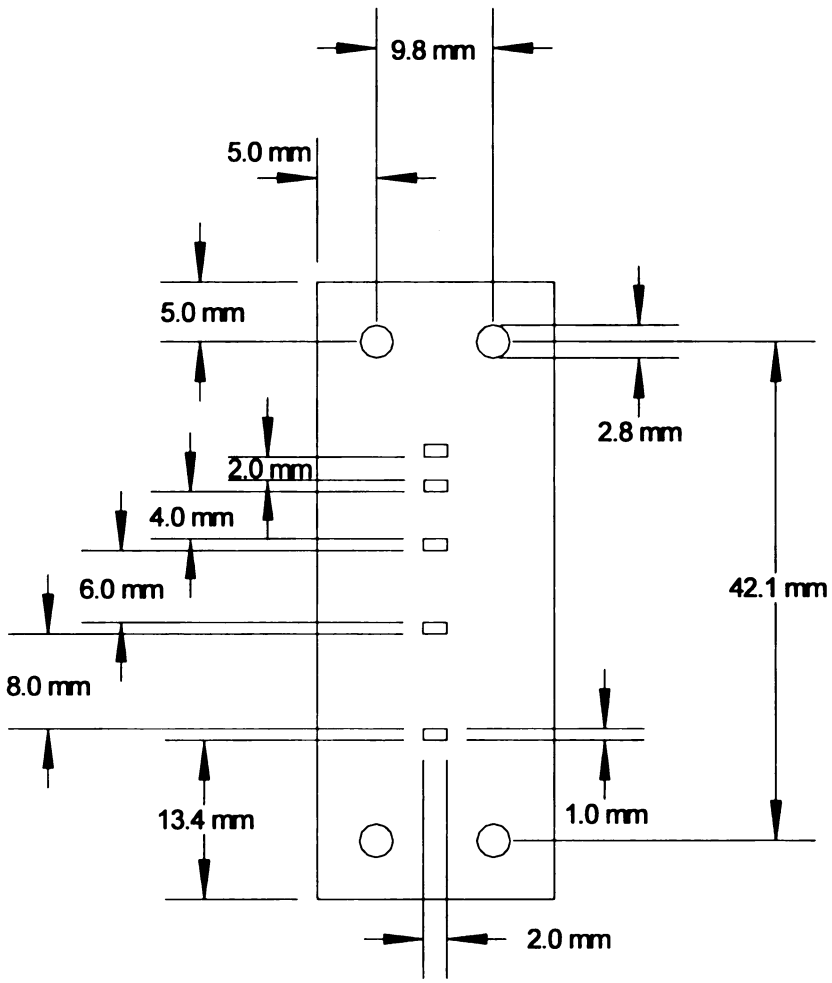

Figure 3: Transmission Line Mask 1

This mask was designed as a shadow mask such that the contact material would deposit only in the ordered pattern needed for the TLM measurements. The contact spacing was varied from 2mm to 8mm in 2mm increments. Each contact has an area of $2mm^2$. The first mask was design not only as the mask, but also doubled as the sample holder. The mast has 4 screw holes at the corners that are used to screw down the mask and also press the sample to the platen. Several challenges with this design were discovered during its use, such as the

need for the sample to be perfectly flat to keep the sample held well in place. Placing and centering the sample while screwing the mask into place was challenging, and the sample had a tendency to crack under the pressure. The mask did serve its purpose well until the second TLM mask was designed. Because of the challenges associated with this mask design, a second design was developed as shown in Figure 4.

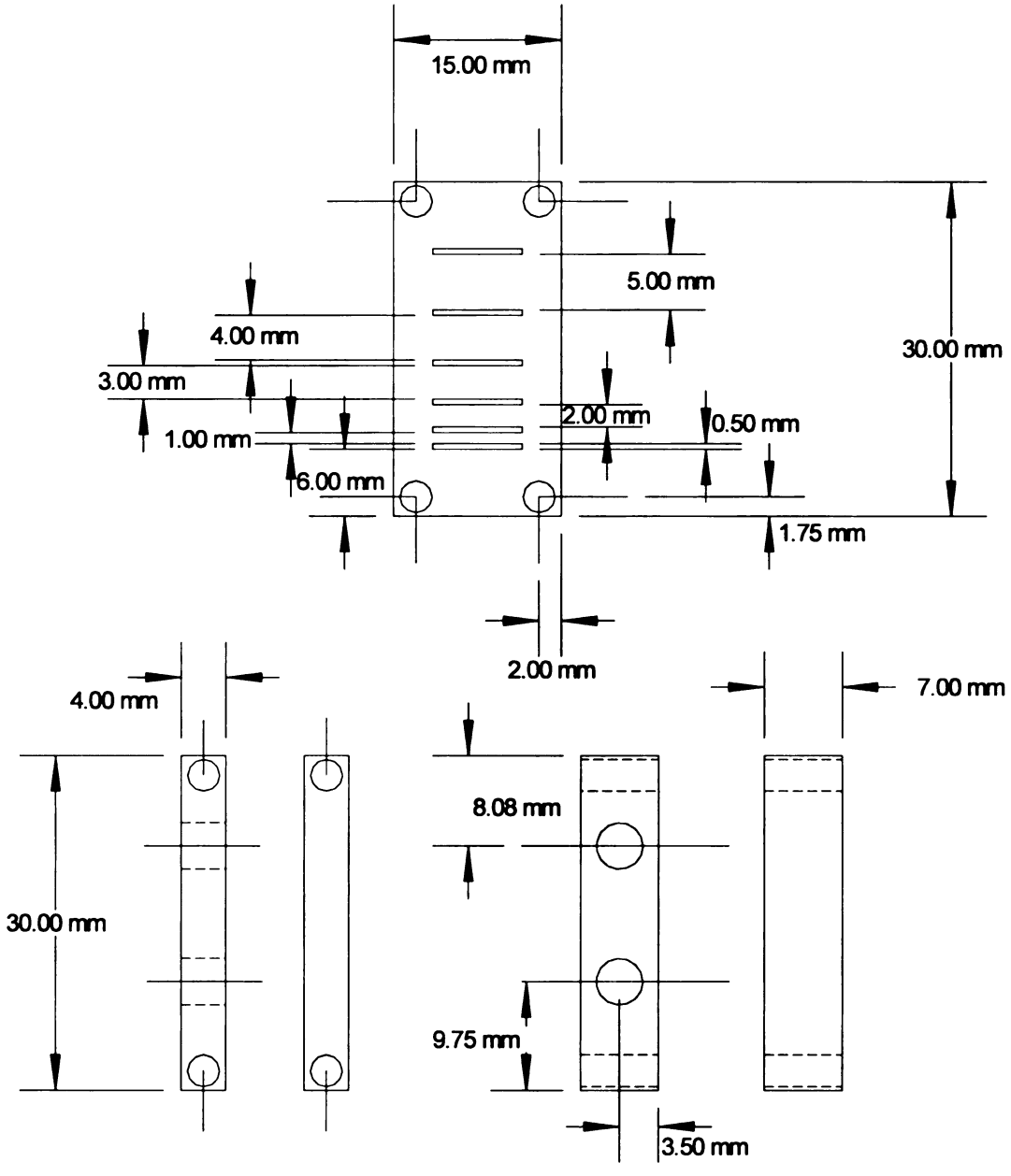

Figure 4: TLM Mask 2

With the 2nd TLM Mask the sample is held in place from the side with a spring-loaded setscrew. The spring would allow for any expansion or contraction of the sample during the deposition. Due to the nature the set screw only making a

small pressure contact, the possibility of cracking the sample while setting it into place is very minimal.

The first mask also presented the problem that the contacts deposited would only have an area 1mm by 2mm. This meant that your sample size could only have a maximum width of 2mm. If the sample had a width larger than 2mm, then current crowding would effect the measurement. With the second TLM mask (Figure 3), many different sample widths could be accommodated. The spacing of the contacts was reduced by a millimeter to allow for shorter samples. More contacts could be deposited per length allowing for better measurements.

Figure 5: Example of deposited contacts to LAST material.

With this new mask, deposition of contacts was sped up, and more data was able to be collected.

Lastly another mask was developed to hold as many samples as possible in order to deposit contact materials. The 32 sample holder was developed to do just that.

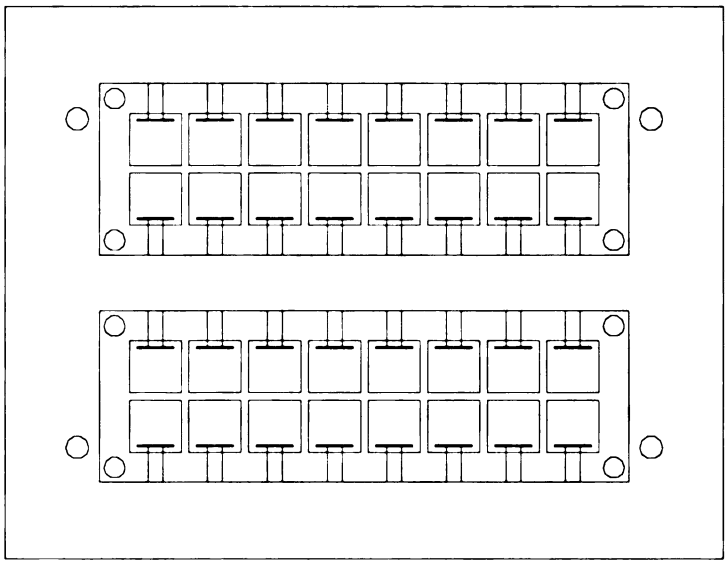

Figure 6: 32 Sample Holder

Figure 5 shows the top view of the 32-sample holder where each sample can be up to 5mm by 5mm in cross section, and as tall as 7mm. Each sample is held in place by a spring-loaded setscrew. The mask is made to allow the user to deposit contacts on one side of the material and the just flip the entire holder over to deposit contacts to the other side. This can be done without removing any of the samples. This makes contact deposition fast and efficient for module fabrication.

3.6 Deposition of Contacts

The first contacts investigated were tungsten which was sputtered deposited onto the LAST materials. Tungsten was chosen due to its good contacts reported to lead telluride [11]. As expected, the sputtering rate for tungsten was found to be very low; however an added difficulty of maintaining the

proper pressure (at least 5mTorr of argon) led us to investigate alternative deposition techniques for tungsten.

3.7 Electron Beam Deposition of Tungsten

Although tungsten has a melting point of 3410°C, it can be deposited by e-beam evaporation. This is possible by focusing the electron beam such that the local temperature exceeds the melting point of tungsten. Because of the high melting point, the current needed (500mA) it higher than typically used (200mA). The deposition rate is relatively low (~ 1.5Å/s), therefore a thin layer of tungsten (20nm) was followed with a thick layer of gold (200nm).

3.8 Initial Contact Measurements

After achieving a good deposition of contacts into the desired pattern, the contacts were tested to verify they were ohmic. To verify a linear current versus voltage behavior of the metal to semiconductor junction, a LabView program was written to control the current through the junction and collect the corresponding voltage data. A diode behavior for the junction would show as a non-linear current versus voltage curve as the current passes through zero. To avoid voltage drops along the measurement cables, a four-probe technique in a Janis cryostat probe station. In the probe station, the environment was pumped down to ~300mTorr. The gold-tungsten contacts were measured with a current between –200mA to 200mA.

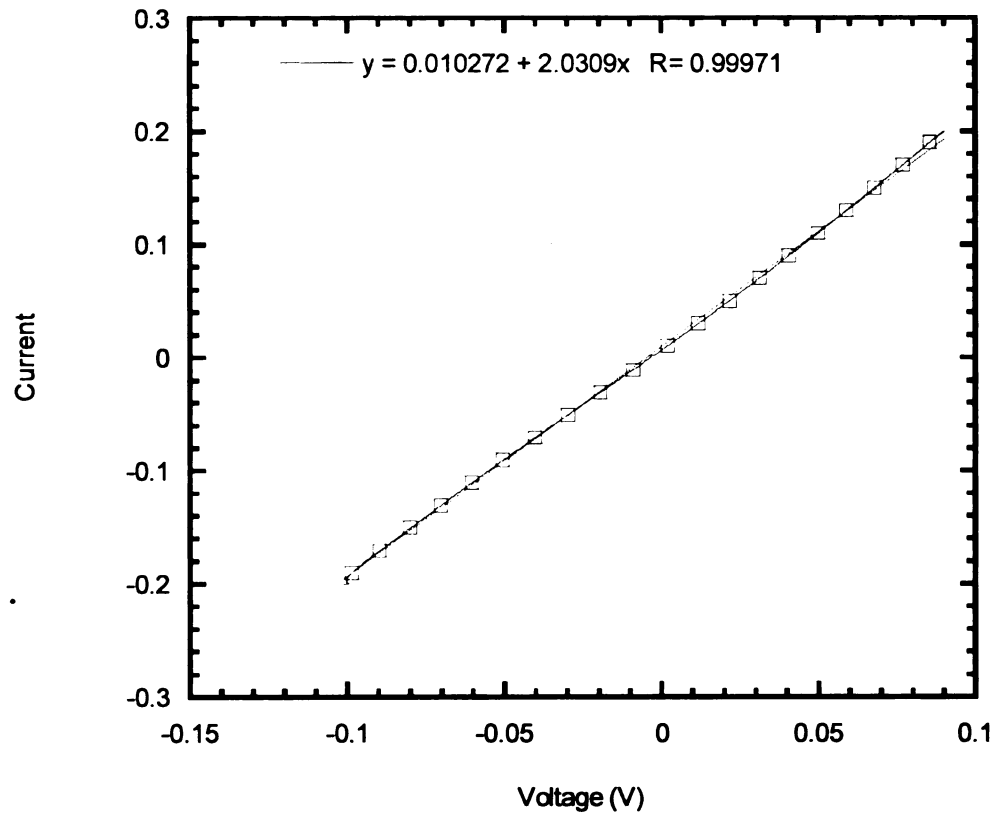

Figure 7: Tungsten-Gold Contact IV

Figure 7 shows the collected data are a good fit to the linear approximation indicating an ohmic behavior for this junction. This came as no surprise as the semiconductors used in this study were doped to high degeneracy.

In the next step resistance measurements between the adjacent contact pads were taken to obtain the contact resistance by the TLM technique. The first contact measurements on an n-type LAST sample (ETN1) came out inconclusive and was believed to be due to inhomogeneities and/or cracks in the sample.

A p-type LASTT sample (ETP2) was then investigated. The conductivity of the sample was measured to be 1,330S/cm and is very uniform. For these contacts a deposition was done of 10nm of tungsten followed by 300nm of gold

and a contact resistance of 119$\mu\Omega cm^2$ was found. This is a good start, but we would like to see contact resistance of close to 5 $\mu\Omega cm^2$ to have good overall module efficiency. To help verify this result, a contact scan just in between each contact pad was also done, and then the difference of the two resistances and divided by two. The contact scan is done with a four probe measurement method. This measurement is also done in the Janis probe station. The measurement is done under vacuum to ensure accurate results. This also gave a contact resistance of around 120$\mu\Omega cm^2$ in good agreement with the results from the TLM technique.

A relatively thick layer of tungsten alone on n-type LAST was investigated next. A thickness of 100nm was deposited at a rate of 1.5Å/s, and a contact resistance of 65$\mu\Omega cm^2$ was measured by the TLM technique. The effects of annealing these contacts were studied next.

3.9 Annealing of Contacts

Annealing of the contacts is needed to help drive the atoms of the contact metal deeper into the bulk material to hope for a lower contact resistance. A good example is that most contacts to silicon are made with aluminum. If this contact is deposited without an annealing step, a Schottky junction at each interface is obtained, however with a high temperature anneal the aluminum to silicon junction becomes ohmic. The tungsten contact was annealed at 600°C for 1 hour.

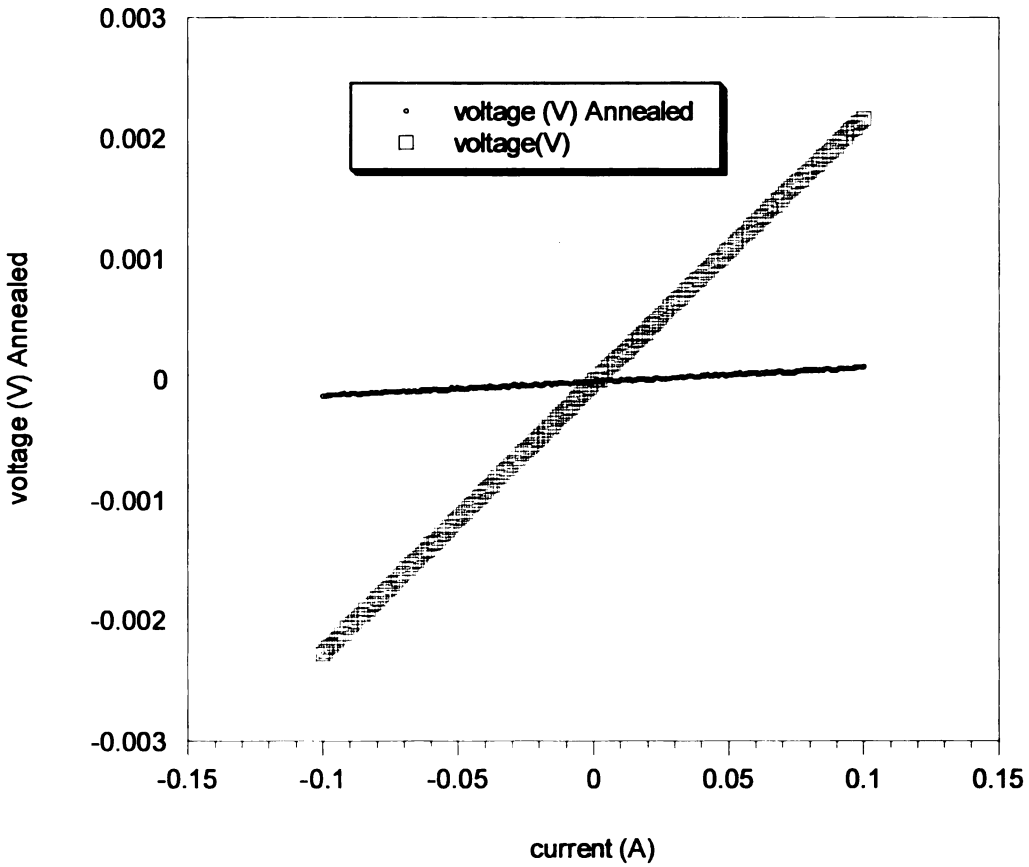

Figure 8: Annealed IV scan vs Preannealed

Figure 8 shows the voltage versus current scan between two contact pads of tungsten on an n-type LAST sample. The curve after a 600°C annealing step shows a significantly smaller slope, indicating a reduced contact resistance. A voltage scan along the sample alone indicated no change in the sample resistance after annealing, thus the improvement shown in Figure 7 is due to the contact resistance alone.

Annealing the tungsten/gold contact at 400°C for 1 hour inside a vacuum sealed quartz tube showed significant degradation of the contacts as shown in Figure 9.

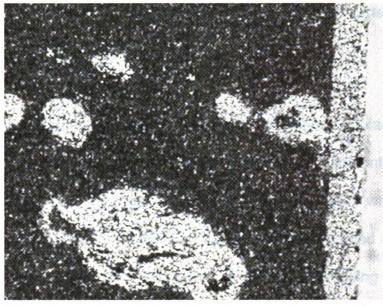

Figure 9: Gold Tungsten Anneal 400ºC 1 hour

More investigation is needed to discover what chemically happened at the contact. Only now assumptions can be made. One being that the gold just absorbed into the sample. Another could be that the gold evaporated completely off of the sample. Lastly that the tungsten and the gold formed some sort of alloy. Once again these are all speculations and need to be verified scientifically.

Chapter 4 Investigating Different Metals for Electrical Contacts

4.1 Antimony Contacts

It was then suggested that antimony might be a good contact material. To investigate this, a 1μm film of antimony was e-beam deposited onto a p-type LASTT sample (ETP2). The TLM measured contact resistance was found to be $56.83\mu\Omega cm^2$. Next, a bond of LASTT to antimony was attempted at the end of the sample (in the configuration that would be used for fabricating a device). A sample of LASTT was placed in a quartz tube with a coin of antimony on top of it and three stainless steel weights were placed on top of the antimony. The stack of materials was placed into a quartz tube and vacuum-sealed as shown in Figure 10. The temperature was raised to 600°C and it remained at high temperature for only a few minutes.

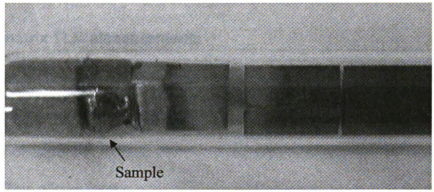

Figure 10: Antimony to LASTT bond. Three stainless steel weights are shown on the right.

As shown in Figure 9, the antimony melted around the sample. The antimony did bond, however the stainless steel weight bonded as well. Next this sample was taken and a cross section was cut to see the interface of the two materials.

Figure 11: Antimony to LASTT interface cross section

There is a clear-cut interface between the two materials. Since the antimony melted during the bonding process, there is good coverage of the LASTT surface. After cutting the sample, the sample size was too small for further contact resistance measurements.

4.2 Cerromatrix TLM Measurements

Diffusion bonding of the hot side contacts is necessary since it will be exposed to temperatures as high as 600ºC during operation. The cold side of the module is not expect to exceed 200 ºC, however also requires low resistance contacts. This allows for the possibility of solder contacts on the cold side. To that end, a Cerromatrix solder was investigated. This solder is similar to Woods metal, and solders very well to the LAST materials. The Cerromatrix was soldered to a piece of LAST into the TLM pattern for contact resistance measurements.

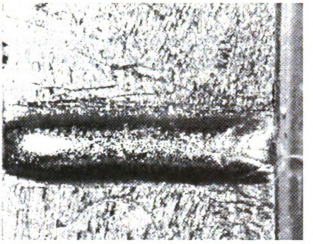

Figure 12: TLM solder contact pad

The contact resistance of the solder to the sample was found to be $33\mu\Omega cm^2$ which is quite good for device fabrication.

4.3 Other TLM material Testing

Although antimony was found to be a promising contact, many other materials were also tested. The following table is good to use a reference for later bonds. All contacts were deposited by electron beam, and measured in the probe station.

Table 2: Contact resistance of different metals to LAST and LASTT samples

N/P	Material	Contact Thickness	Contact Resistance ($\mu\Omega cm^2$)
P	Sb	1μm	80
N	Sb	1μm	20
P	Ag	500nm	500
N	Ag	500nm	1800
N	Cr	500nm	275
P	Cr	500nm	120
N	Ti	250nm	130
P	Ti	250nm	145
P	W	100nm	65
P	W/Ag	20nm/200nm	140

Contact metals were chosen along the lines of what was attempted in the literature [14]

Chapter 5 Bonding of Contacts to Thermoelectric Material

5.1 Diffusion Bonding

Diffusion bonding is a system of bonding two similar or dissimilar metals, alloys, or nonmetals. This is achieved by pressing the two materials that you would like to be bonded, preferably under vacuum or in the presence of an inert gas to reduce oxidization. There are three elements that control how well the bond is formed; first is the temperature you are doing the bonding at, second is the amount of weight is placed onto the samples as pressure keeping the two interfaces together, and lastly is the amount of time you stay at a certain bonding temperature. The bonding temperature should be anywhere to 50-70% of the melting point of the most fusible metal. The temperature aids in the inter-diffusion of the atoms across the interface. The bonding pressure fills voids and pushes out any oxides that may reside on either of the two surfaces. The time of bonding needs to be minimized. If the bonding time is too long, voids will be created at the interfaces, and chemical changes may occur.

In the case with LAST we are looking to reduce the sizes of the grains in our system in order to create higher density samples [12]. Diffusion along grain boundary paths becomes the dominant diffusion channels. So in our attempts to decrease the grain size of our materials we will greatly improving the diffusion bonding of our interfaces, yielding a reduced contact resistance and better overall efficiency of our module. The increase in grain boundaries is a case in which the ease that the atoms can migrate along the free surfaces of the grain boundaries.

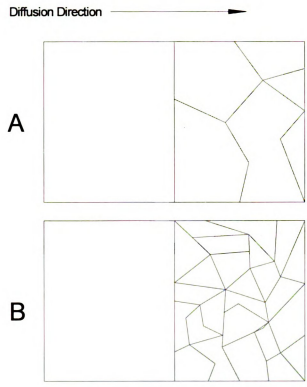

Figure 13: Diffusion bond B will have better interface resistance due to the reduction in the size of the grain boundaries.

Diffusion bonding attempts were done at many different temperatures, pressures, and times. Along with good bonds, we also wanted to make sure that we did not degrade our samples at the same time (through desorption of the sample) Such desorption would degrade the properties of the sample and result in a decrease the performance of the device. To minimize this outgassing of material, the diffusion bonding was done in an overpressure environment of argon.

5.2 SnTe Diffusion Bond

Tin telluride was the first alloy investigated for bonding to LAST. The alloy was prepared in the Chemistry Department and then vacuum-sealed in a quartz tube, with small quartz weights placed on top. The bonding temperature was raised at a rate of 50 degrees a minute to 550°C and then slowed to a rate of 20 degrees per minute to 700°C. It was maintained at the maximum temperature for a few minutes, and then the furnace cooled over night.

When first investigated the bond appeard to have bonded well with no signs of outgassing.

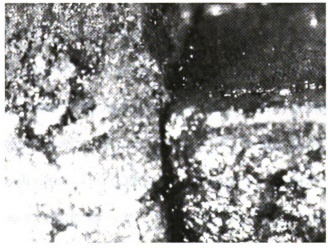

Figure 14: SnTe interface with the LAST

After opening the quartz tube, however we found that there really was no bonding of the alloy to the LAST. From this experiment, it was hypothesized that one or more of the following conditions were needed for better SnTe-LAST bonds:

- Increase bonding temperature

- Increase pressure between materials during bonding
- Increase the time of the bonding

5.3 Nickel Antimony Bonds

Based on the earlier results that showed good contact between antimony and LAST, but too low of a melting point for antimony, we investigated a small amount of antimony between the sample and a metal interconnect. To choose the metal interconnect materials with good resilience to oxidization, low electrical resistivity, and a coefficient of thermal expansion well matched to LAST were sought. Nickel has such characteristics, along with a relatively high thermal conductivity for good transfer of heat into the module, and it is readily available to purchase. To test the bonding characteristics of antimony to nickel, pieces of antimony and a nickel pellet were vacuum sealed in a quartz tube and annealed at 700°C for a few minutes. The quartz tube was then removed from the crucible furnace and allowed to naturally cool. The antimony was found to bond well to the nickel with good coverage and wetting characteristics similar to a solder.

Next a bond between the antimony coated nickel and a sample of LAST material was investigated. The two pieces were again vacuum sealed into a quartz tube and annealed at 700°C for a few minutes. It was found that the antimony coated nickel bonded well to the LAST material, however there was excess antimony in the structure that would hinder device fabrication. Therefore, thin film depositions of antimony were investigated. .

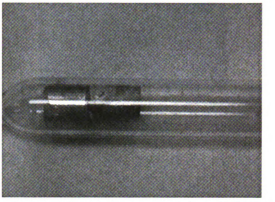

Figure 15: Nickel antimony alloy bonded to LAST

5.4 Antimony Thin Film Diffusion Bonding

To begin an n-type sample of LAST (ETN16) was loaded into a mask, and placed in the physical vapor deposition system located in the Engineering Research Complex Cleanroom, and the chamber was pumped down to ~10^{-6} Torr.. Argon was then allowed to flow into the chamber to a pressure of 100mTorr, and a plasma etch of the sample was initiated to remove oxides and hydrocarbons from the sample surface. Then the chamber was evacuated again, and 500nm of antimony was e-beam deposited onto the sample. A nickel electrode was then polished to clean mirror finish with 2,500 grit sandpaper. The antimony coated LAST sample was then bonded by loading them into a vacuum sealed quartz tube and raising the temperature to approximately 700°C. The bond attempt was successful as shown in Figure 16.

Figure 16: Antimony thin film to nickel diffusion bond. In this photo, the sample was mounted in cutting wax.

To study the temperature dependence of the contact resistance during annealing, the sample was mounted with electrical current and voltage leads in a standard four probe configuration as shown in Figure 16. The sample was mounted in the Ultra High Temperature (UHT) measurement system and the junction conductance was monitored during annealing under a vacuum.

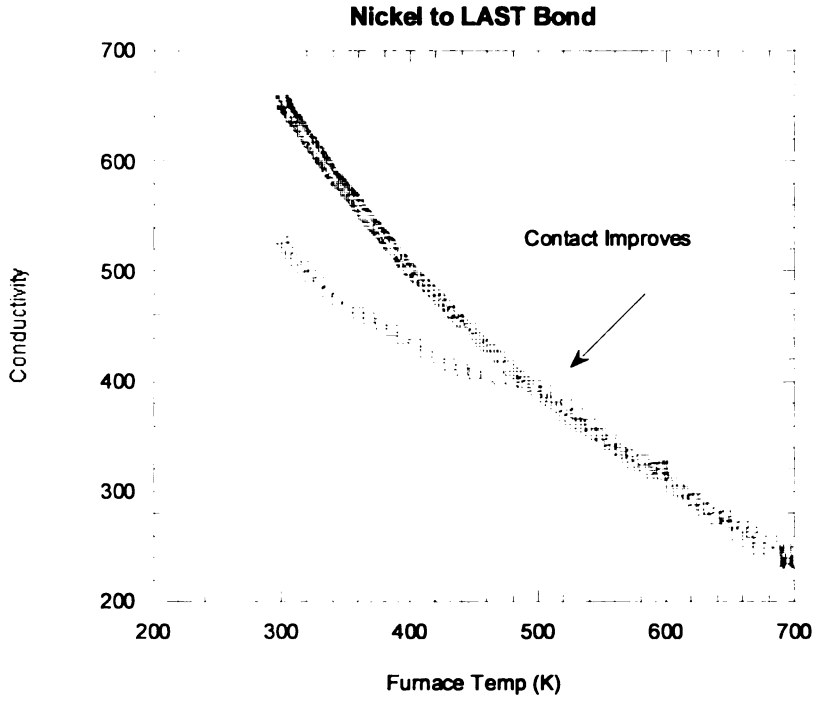

Figure 17: Annealing data

As seen from the data (Figure 17), near 500K the conductivity curve changes slope. This is showing an improvement of the contact at this temperature. The conductivity then continues on this trend to 700K, and overlaps the 500K data upon cooling. Thus a high diffusion of antimony atoms near 500K appears to significantly improve the contact during annealing. It should be noted that no pressure was applied to this contact during annealing.

5.4.1 TLM Measurement of Nickel Antimony Contacts

Using the TLM mask 500nm of antimony was deposited onto an n-type sample of LAST followed by 150nm of nickel.

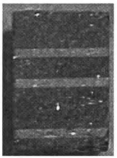

Figure 18: TLM contacts of Ni-Sb on LAST

The contact resistance measured is $140\mu\Omega cm^2$. This is still too high to build an efficient device. The sample was then vacuum-sealed into a quartz tube and annealed at 700K for 39 hours. The contact resistance improved after the anneal to $16\mu\Omega cm^2$ which was very encouraging. With a contact resistance this low, it can be considered negligible when fabricating a device.

Figure 19: TLM contacts after anneal

The contacts darkened some during the anneal, but there was no apparent change in the LAST and contact metal. The fact that the tube is a small environment, during the annealing process, anything that does outgas would create an overpressure. Thus it could be possible that an equilibrium is established that would keep the material from outgassing further. With this low of a contact resistance, it was time to begin building devices. At this time we had no system that was large enough to build modules. All diffusion-bonding attempts up to this point were done in tiny vacuum-sealed quartz tubes. An entire module will not be able to be sealed individually and then baked, so the fabrication of a diffusion furnace was needed which could accommodate the size of the modules planned for the final devices.

5.5 Other Bond Experiments

Two other experiments assocated with the bonding are also worth noting. First was to do EDS analysis on the interface between the nickel and antimony,

by first removing the nickel electrode. This interface is shown in Figure 19 after removal of the nickel electrode.

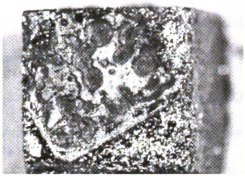

Figure 20: Antimony-LAST interface after bond

The EDS showed the interface was tellurium rich. After subsequent EDS analysis on other samples, this was common to find tellurium at the contact and on other surfaces of the electrodes.

An attempt at a nickel antimony diffusion bond was done in open air. The result was that both samples turned black from oxidization and no bond occurred. The conclusion is that the bond must be done in an oxygen free environment to ensure a good bond.

Next a bond of tin to LAST was investigated. Since tin has a low enough melting point, a soldering iron was used to apply a layer of tin to the LAST material. From this simple connection technique, a contact resistance of $79\mu\Omega cm^2$ was found. Since tin was thought to be a p-type dopant for these materials, there was concern of using tin on the LAST materials, and future experiments focused on tin to LASTT p-type samples.

Chapter 6 Diffusion Furnace

6.1 Designing a Diffusion Furnace System

A three zone furnace was utilized in the design of this system to help obtain a uniform temperature region in the center of the furnace. The size of the furnace was chosen to accommodate several large thermoelectric generator modules and/or the individual unicouples for such modules for simultaneous diffusion bonding of the contacts. Based on this a center zone of 12 inches long and the two outer zones 6 inches long was chosen. The bore size of the furnace was chosen to accommodate two or three modules side by side requiring a bore size of at least 5.125 inches in diameter.

To control the environment around the modules during bonding, a quartz tube was included in the design, and the length of the tube was chosen such that o-ring seals at the ends of the tube could be made without the need for water cooling. To accomplish this, the quartz tube was selected to extend an extra two feet out each end of the furnace (8' quartz tube in total length).

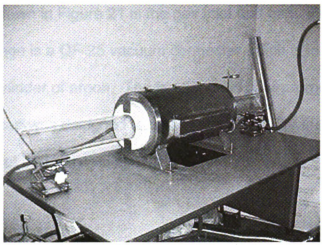

Figure 21: Diffusion furnace with quartz tube

The endcaps for the quartz tube were designed to be easily removable, provide a vacuum seal of lower than 10mTorr, to be relatively light, and to have gas inlets and vacuum ports to control the environment in the chamber. In addition, there was interest in investigating diffusion bonding at atmospheric pressure of argon. To maintain the position of the endcaps during backfilling of the argon, a structure was built with angle brackets to keep the end caps in place as shown in Figure 22.

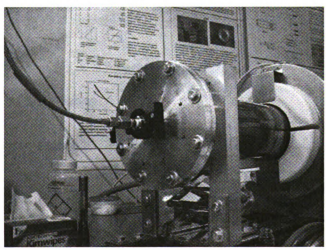

Figure 22: Gas inlet end cap

The end cap shown in Figure 21 is the gas inlet end cap. Welded to the 6 inch aluminum iso-flange is a QF-25 vacuum connecter which is in turn attached by a ¼ gas line to a cylinder of argon. The iso-flange is easily removed with eight bolts. The end cap was designed to seal to the outside of the quartz tube by compression of a set of o-rings as shown in Figure 23.

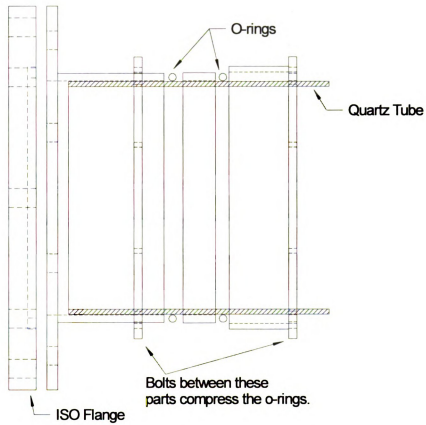

Figure 23: Endcap design exploded view.

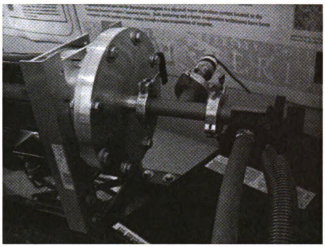

Figure 24: Vacuum connect end cap and pressure gauge attachment

The vacuum port end cap mirrors that of the inlet, but connected to this end is the vacuum pump, TC pressure gauge, and a valve. The vacuum pump is a tri-scroll dry roughing pump with a base pressure of around 10mTorr. The valve is used to seal the system and allow the furnace to run independent of a vacuum pump. This is used when the tube is filled with a gas and an overpressure is desired.

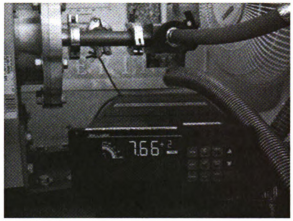

Figure 25: TC gauge for diffusion furnace

The thermocouple gauge is used to monitor the pressure inside the quartz tube. After backfilling the quartz tube with argon, the thermocouple vacuum gauge becomes inaccurate. This is due to the change in the thermal conductivity of the gas in the furnace. The proper trends are still read by the gauge, an example being the pressure rising and falling during heating and cooling. Occasionally the bolts that squeeze the o-rings need to be retightening to keep a good seal. Also added to the end of the quartz tube is an o-ring used as a cushion to keep the aluminum iso-flange from chipping the very end of the quartz tube during vacuum (a soft bump for the quartz tube). To test the vacuum seals to the quartz tube, a base pressure of 3mTorr was reached, and the system was then valved off and found to be able to sustain vacuum over night.

The furnace temperature controller consists of three PID controllers (one for each zone) which regulate the power to each zone through a three phase solid state relay. The controllers receive the input by three type K thermocouples placed in the center of each of the three zones.

Figure 26: Temperature Controllers

The controllers can be set to slowly increase temperature at a user selectable ramp rate, and a desired soak time. This makes the furnace very easy to operate, and does not need to be watched during a run. It is good to make note of the pressure periodically, and to keep the end caps cool during the diffusion process by a fan. Desorbed material during diffusion collects on the colder regions of the quartz tube just outside the furnace, however the center zone remains relatively clean due to the low sticking coefficients at the higher temperatures of the center zone.

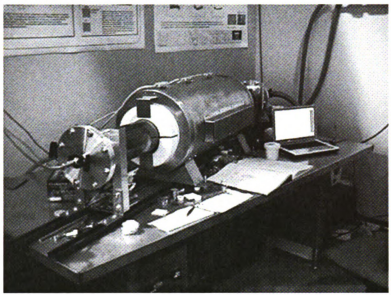

Figure 27: Overall diffusion bonding system showing the quartz tube, the inlet endcap, and the thermocouples for each zone on top of the furnace.

For added safety, a stainless steel top for the table on which this diffusion furnace system sits was fabricated. Also, within the quartz tube, circular disks of stainless steel were inserted to further insulate the center zone, and help to maintain a more isothermal region in the center. This was found to be particularly helpful with such a large diameter quartz tube chamber.

6.2 Unicouple Boat

To place the thermoelectric materials inside the diffusion furnace and bond them to the electrodes, a quartz "boat" was designed. While the system is capable of bonding an entire module in a single run, if any of the legs forms a bad contact or cracks during the diffusion process, the entire module will be inoperable. By designing a quartz boat individual unicouples could be fabricated, and tested before assembling into the final module.

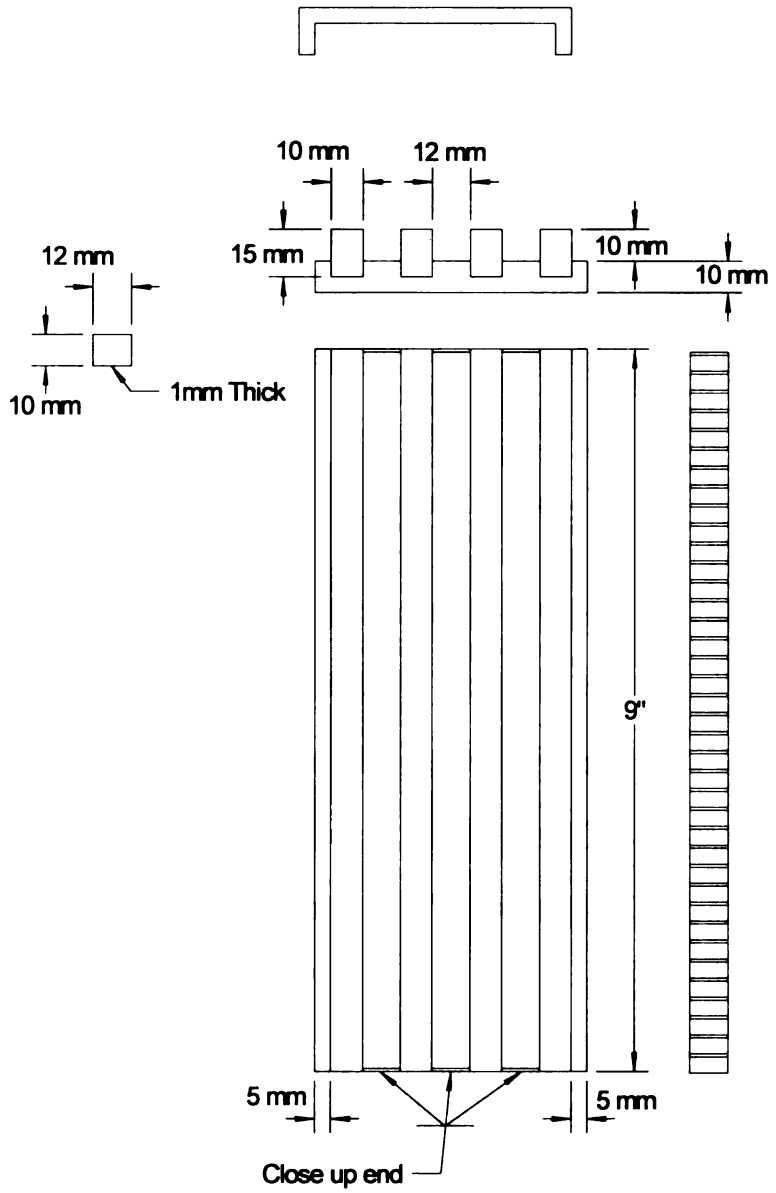

Figure 28: Preliminary drawings for unicouple boat

The boat was designed to hold up to 140 unicouples at once to rapidly fabricate many unicouple in a single diffusion run.

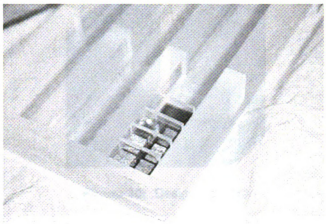

Figure 29: Unicouple Boat

The boat also makes it easy to run many different experiments at the same time. It is large enough to separate different bond attempts so that one bond will not contaminate the other. The only negative aspect of this boat is that it is fabricated to only hold one size unicouple, 5x12mm. If the sizes were to change a whole other boat would have to be built. This unicouple boat still does serve its purpose well.

6.3 Furnace Run 1

For the first run six n-type and six p-type samples were first dipped into a ZnCl solution and then placed into an antimony powder. The ZnCl was used as a flux to aid in the bonding process.

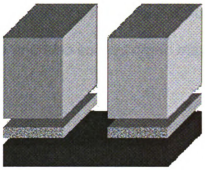

Figure 30: Design diagram

The samples were placed onto nickel strips and then placed into the furnace for bonding. The furnace was pumped down to a base pressure of around 10mTorr, and then argon was allowed to flow into the chamber at a constant rate of 5 liters per minute. The furnace was raised to 650ºC. The whole run had a continuous flow of gas, and the overall pressure of the system never got above 3Torr. After the furnace sat at 650ºC for about 10 minutes, the temperature was set to 22 ºC and allowed to cool over night.

No bonds resulted. The materials also out gassed and changed colors.

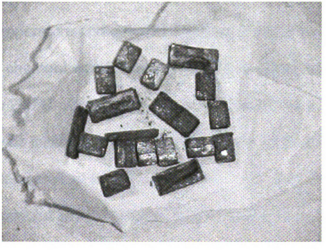

Figure 31: Run 1 results

The nickel also changed to a pinkish color. The conclusion was that the run was done at too low of pressure and also some oxygen may be leaking into the system.

6.4 Experiment 2

The second bonding experiment did not use an antimony powder, but a bar of antimony about 0.5mm thick.

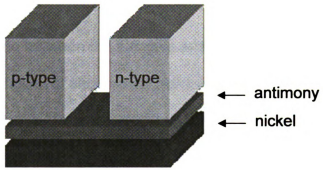

Figure 32: N and P material to antimony bar all to a nickel strip

This experiment resembles the first nickel antimony bonds, however here it was done at a lower temperature and a higher pressure to minimize outgassing from the samples. The chamber was first pumped down and then the furnace was set the temperature to 250°C. Once the furnace reached 250°C a flow of argon gas into the chamber was initiated to raise the pressure to 300Torr and then sealed off the tube. The temperature was then raised to 575°C and maintained there for approximately 10 minutes before cooling to room temperature over night.

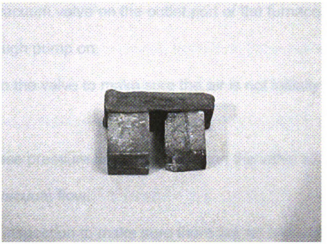

Figure 33: Bonded unicouple with antimony bar to nickel

As seen in Figure 33, a bond between the samples and the electrode was formed. The contacts did, however show some signs of roughening, and flakes of metal could be easily removed from the electrode. The higher pressures were found to be helpful for preventing outgassing from the LAST and LASTT materials.

6.5 Furnace Operation

After a few runs of the furnace, it became apparent that many of the same routines were being repeated, with only small changes in pressure, maximum bonding temperature, and bonding time. The following is a list of general instructions to operate the diffusion furnace.

1. Load samples for bonding into boat and then place into the center of the hot zone in the furnace.
2. Bolt the iso-flange in the order specified on the front of the flange.
3. Attach the gas line from the cylinder to the front of the iso-flange.

4. Close the vacuum valve on the outlet port of the furnace.
5. Turn the rough pump on.
6. Slowly open the valve to make sure the air is not initially evacuated too fast.
7. After the base pressure begins to fall, open the valve all the way to ensure maximum vacuum flow.
8. Do a quick inspection to make sure there are no leaks in the system.
9. Let the furnace pump down for about an hour, or until a pressure of near 20mTorr is reached.
10. Turn on the gas flow and open the cylinder and allow gas to flow through the furnace. This process will help sweep away oxygen, water, and hydrocarbons that remains in the tube.
11. While the gas is flowing, set the temperature controllers as follows
    a. Hit the scroll key once to set point 1
    b. Hit enter
    c. Set the desired maximum bonding temperature
    d. Hit enter, and the controlled will display, "stored"
    e. Scroll to "config" and hit enter
    f. Scroll to "ramp" and enable it
    g. Enable soak
    h. Then enter the desired ramp time. The controllers are programmed to input the total time to reach the maximum temperature in hours and minutes

i. Enter the soak time in hours and minutes

j. The controllers are now set, and when the run is completed it will automatically shut off your furnace.

12. Allow the gas to flow for about 3 minutes, then shut the vacuum valve completely and turn off the scroll pump.
13. Let the inert gas fill the chamber till it has reached the desired starting pressure. It has been found that above 300Torr samples show little outgassing during the run.
14. Turn off gas flow and close cylinder valve.
    a. It takes at least 8 to 10 hours for the furnace to completely cool, so it is good to put runs in during the afternoon so the furnace is cool the following morning.
15. When the furnace has cooled to a reasonable temperature (below 70°C) turn the vacuum back on and open the outlet valve.
    a. This procedure is done to pump out residuals that may reside inside the furnace that are not safe to breath.
16. Close vacuum valve
17. Shut pump off and remove vacuum hose
18. Open outlet valve slowly to allow the furnace to vent
19. Once back to atmosphere, carefully remove the inlet iso-flange and remove the sample boat.

This procedure has also be utilized for sintering and thermal etching of samples.

6.6 Diffusion Bonds and Results

The following is a list of bond attempts and results of those different bonds. Photos were taken of each bond, and are available in the appendix.

Table 3: List of diffusion bonds and results

Bond Investigated to LAST	Temp (°C)/ Time (min)	Pressure Ar_2	Visual Inspection
$ZnCl_2$ pre-etch + Sb powder	650/10	300mTorr	No Bond (out- gassing)
Sb	622/10	29Torr	Good Bonds (no out-gassing)
Bi/Sb (55/45) on Ni	500/10	200Torr	No Bonds
Bi/Sb only	500/10	300Torr	Good Bonds
Bi/Sb to Ni (No LAST)	500/10	300Torr	Bi/Sb blackens on Ni
Sb only	604/10	200Torr	Good bonds
Sb on Ni (No LAST)	604/10	200Torr	Not Bad- a little blackening
Bi/Sb (55/45) on Ti (No LAST)	500/10	215Torr	Good bond between metals
Bi/Sb (55/45) on W (No LAST)	500/10	215Torr	No bond between metals
In (0.5mm thick) on Ni	640/10	215Torr	Consumed Samples
In on Ni (No LAST)	500/10	215Torr	Good Bond between Metals
In on Ni (prealloyed)	650/10	580Torr	Good Bond
In 1μm thick on Ni	640/10	450Torr	Good Bond
Stainless steel	755/240	250Torr	Well Bonded

Indium was found to bond well to LAST with a low contact resistance, therefore more investigation was done to fabricate unicouples using a thin films of indium between the samples and a nickel electrode.

Chapter 7 Module Fabrication

7.1 Indium Thin Film Modules

One of the better mechanical and electrical contacts that has been found is the thin film indium contact. A 1μm of indium was e-beam deposited onto nickel electrodes as shown in Figure 34.

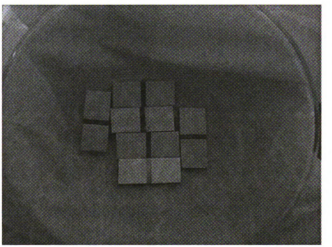

Figure 34: Indium thin film on nickel

Indium has a low melting point of 157ºC and can be easily deposited as thick films. The solid stripe down the center of the nickel electrodes in Figure 34 is where the mask was holding down each individual nickel strip. Bonds formed with indium to LAST were found to withstand temperatures >600ºC suggesting that an indium compound is chemically forming at the contact during bonding.

The bonding temperature for fabricating the unicouple was set to 630ºC and pressure in the furnace was set to approximately 300Torr. When the run was completed, the nickel strips were found to be well bonded to the LAST and LASTT legs. To complete the electrical connections, nickel electrodes were

soldered to each leg at the cold side junctions the Cerromatrix solder supplied from McMaster Carr.

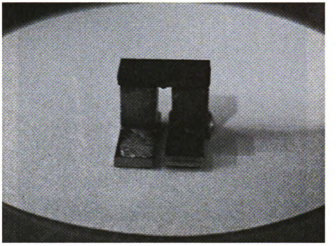

Figure 35: Indium-Nickel unicouple

The module resistance was measured to be 10mΩ. During this measurement, the electrical current was rapidly flipped from positive to negative current values to avoid any thermal offset voltages. With an estimated 3mΩ per leg, the contact resistance is approximately 33% of the total resistance of the module. The contact resistance is such a high part of the module because the total resistance is only 10 mΩ.

7.2 Initial Module Fabrication

Utilizing the indium bonding results, a larger module was investigated consisting of 18 n-type legs and 18 p-type legs in a 4" x 4" configuration. The hot side and cold side electrodes were made of nickel strips as shown for the cold side in Figure 36. Each nickel strip used in the module went through a two stage

polishing process; a 1000 grit sandpaper followed by 2500 grit sand paper. The hot side nickel strips had 1μm indium deposited to them in the PVD.

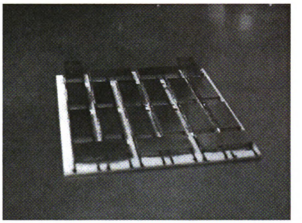

Figure 36: Cold plate and interconnects

The nickel strips were bonded to an alumina plate using silver paste which was cured on a hot plate to form stronger bonds.

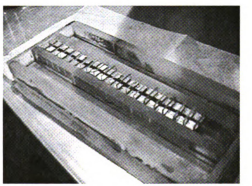

Figure 37: Unicouples in boat before diffusion bonding

Twenty unicouples were assembled into the boat and separated by quartz slides. As done previously with this bond, no weight was added to aid in the diffusion process. For this bonding run the furnace was initially raised to 150ºC under vacuum to help desorb moisture and residual hydrocarbons. At 150ºC the vacuum valve is closed and argon was allowed to flow into the chamber to raise

the pressure to 200Torr. The furnace was then set to 628ºC, however the temperature overshot to approximately 650ºC. Then the furnace was set back to room temperature.

The following morning when the unicouples were taken out of the furnace, a discoloration of the p-type legs (yellow tinge) was noticed as seen in Figure 38.

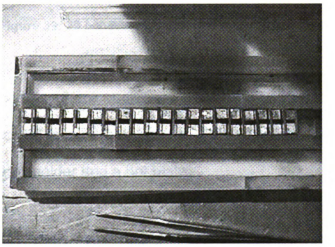

Figure 38: Unicouples after removal from the furnace

The sample yellowing was believed to be caused by excess tellurium that outgassed from the LASTT during bonding. Following this initial investigation the unicouples were removed from the boat to find that all 20 of the unicouples formed bonds.

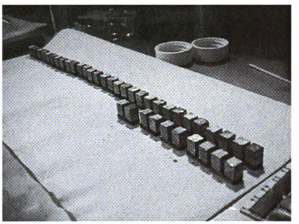

Figure 39: 20 bonded unicouples for module fabrication

To complete the module 18 unicouples were soldered to the nickel strips previously silver pasted to the alumina plate. This cold side bond was formed using the Cerromatrix solder and a hot plate.

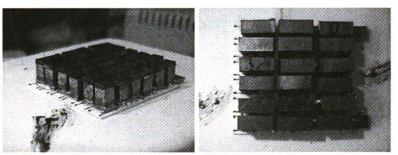

Figure 40: Module fabrication on the hotplate

To help maintain the position of the legs, quartz spacers between unicouple were used. Once this fabrication was completed, the hotplate was turned off to allow the solder junctions to cool. Using an alumina epoxy (Resbond) which cures at room temperature, the top plate (hot side) of the module was bonded to the unicouples as shown in Figure 41.

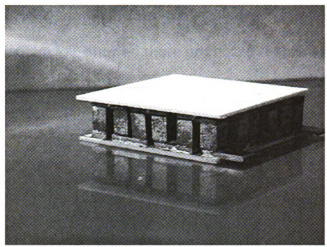

Figure 41: Completed Module

Initial open circuit testing with a temperature gradient of 176K, the voltage the module supplied was 407mV. With the 36 legs we got an estimated thermopower is 98.4μV/K per leg. This number is very close to the expected room temperature thermopower. Additional testing revealed that the bond between the silver and the alumina plate was weak, and after the cold side alumina plate came off, then several of the hot side junctions also mechanically failed.

7.3 Indium Foil Modules

To reduce the fabrication time, an investigation of using a thin indium foil between the sample legs and the nickel electrodes was initiated. This was to be used in place of the e-beam deposition step. A 50μm thick indium foil. Using the foil instead of doing a complete deposition would save entire day on module fabrication. Following the same procedure as for the previous run the results

showed significant reaction with the sample as shown in Figure 42. Using smaller pieces of indium foil, showed more promising results as shown in Figure 43.

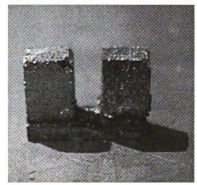

Figure 42: Indium foil bond

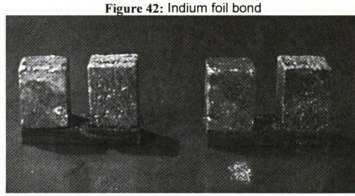

Figure 43 : Indium foil bond small pieces

The two unicouples from Figure 43 were put together into a four leg module as shown in Figure 44. The resistance of the module was found to be 16.82mΩ. This would give each unicouple an estimated resistance of 8.4mΩ, which is lower per unicouple found for the e-beam deposited thin film indium modules.

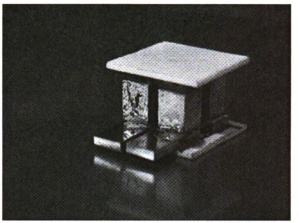

Figure 44: Module formed from the unicouples shown in Figure 43.

Based on these results, a scaled up attempt to fabricate larger modules was made.

7.4 Indium Foil Module Run

The samples and nickel strips were prepared the same way as for the thin film indium module. For this run 30 unicouples were put into the furnace to be bonded.

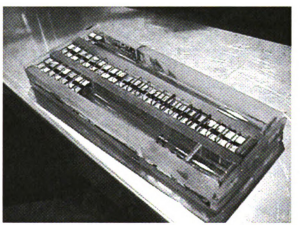

Figure 45: Indium foil module pre-bake.

The same temperatures and pressures were used as before, however only 12 out of the 30 unicouples bonded this time. Between runs, one adjustment to the composition was made to reduce the amount of tellurium outgassing. With the 12 unicouples left, six 4 leg modules were made as shown in Figure 46.

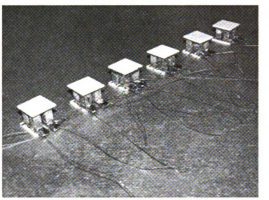

Figure 46: Modules made with left over unicouples

Tests were done on the modules resistances with the results shown in Table 4.

Table 4: 4 Leg unicouple resistances and calculated contact resistances.

Module #	Total Resistance mΩ	Calculated Contact Resistance $\mu\Omega cm^2$
A2	17.8	160
B2	270.2	8078
C2	19.7	205
D2	25.4	396
E2	28.1	570
F2	36.6	798
G2	281.9	8432

Further tests are being initiated to investigate these contacts while the unicouple is under mechanical pressure during bonding.

To better investigate the individual bonds, a scanning probe system was developed to incrementally measure the voltage drop along the sample and across the junction.

Chapter 8 Diffusion Bonded Contacts Investigations and Alloy Bonds

8.1 Improved Contact Resistance Measurement System

As the amount of bonds attempted grew in numbers, the contact resistance needed to be test as well. The TLM method would not work for these materials since they are not bonding in the proper configuration for the TLM measurement. To measure the contact resistance for these bonded junctions, a voltage scan across the contact was needed. Already in use in the lab was a room temperature scanning probe that was used to measure electrical conductivity of materials. It was designed to measure voltage vs. position and with the proper dimensions electrical conductivity is calculated.

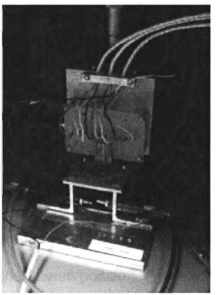

Figure 47: Room temperature scanning probe

This sytem was further tested, and a significant improvement in the measurements was found by repositioning the low voltage pin of the nanovoltmeter used. Positional resolutions as fine as 10 microns could be made,

however to scan across the sample this required a significant number of measurements. Sufficiently good results were found for scan steps of 100μm as shown for a solder to LAST junction in Figure 48.

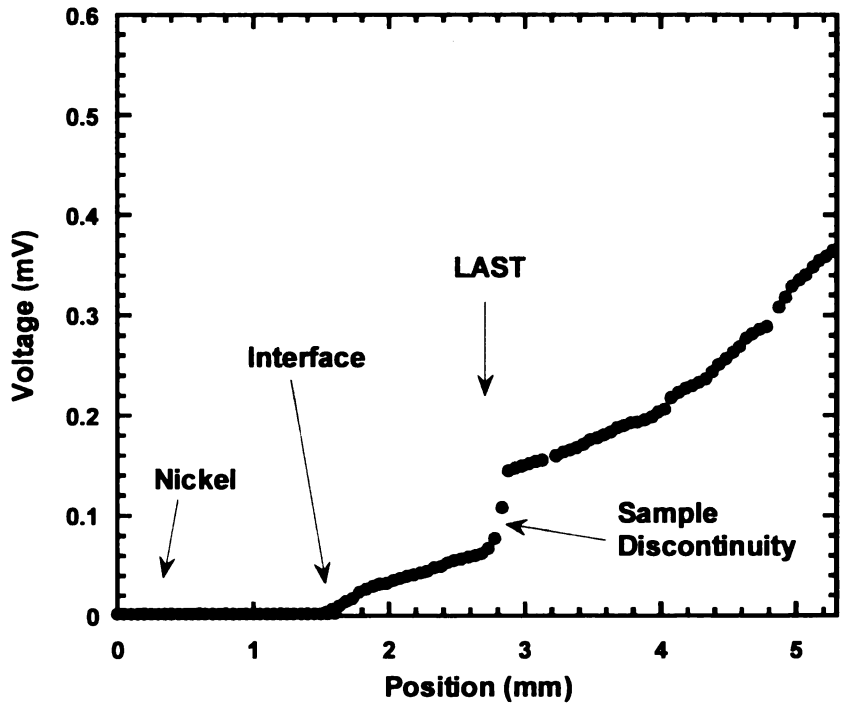

Figure 48: Room temperature probe scan at 100μm resolution across a solder to LAST material junction.

A discontinuity in the surface of the sample at the 2.8mm position can be clearly seen in Figure 48, however the voltage profile at the junction is smooth with a negligible discontinuity at the 1.5mm position. This method has been utilized to measure all contact resistance values for diffusion bonded contacts. In addition to the indium studies described above, several other contacts were investigated.

8.2 Indium Antimony Alloy

A 50-50 weight percent alloy of indium – antimony was fabricated by by a fellow colleague (Jarrod Short). The alloy was cut to approximately 5mm × 12mm × 1.5mm thick, and bonded at a temperature of 500°C and a pressure of 338Torr. The resulting bond is shown in Figure 49 where it can be seen that the alloy melted around the LAST and LASTT legs, and discolored with a black coating.

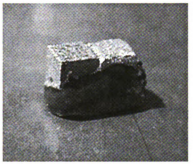

Figure 49: 1st alloy diffusion bond

8.3 Silver Diffusion Bonding

Early measurements by the TLM technique showed contact resistances between silver and n-type LAST of approximately $500\mu\Omega cm^2$ for un-annealed contacts. This experiment was to investigate the effects of bonding at a higher temperature with silver. The silver was bonded at a temperature of 650°C, and above atmospheric pressure of argon.

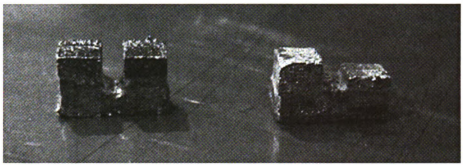

Figure 50: N and P bonds to silver

The results shown in Figure 50 show that the LAST and particularly the LASTT were partially dissolved by the silver. The n-type held up to the bonding process a little better, but also shows signs of deterioration near the silver. Scanning probe measurements across the silver to LAST junction are shown to have very high contact resistivity values as show in Figure 51.

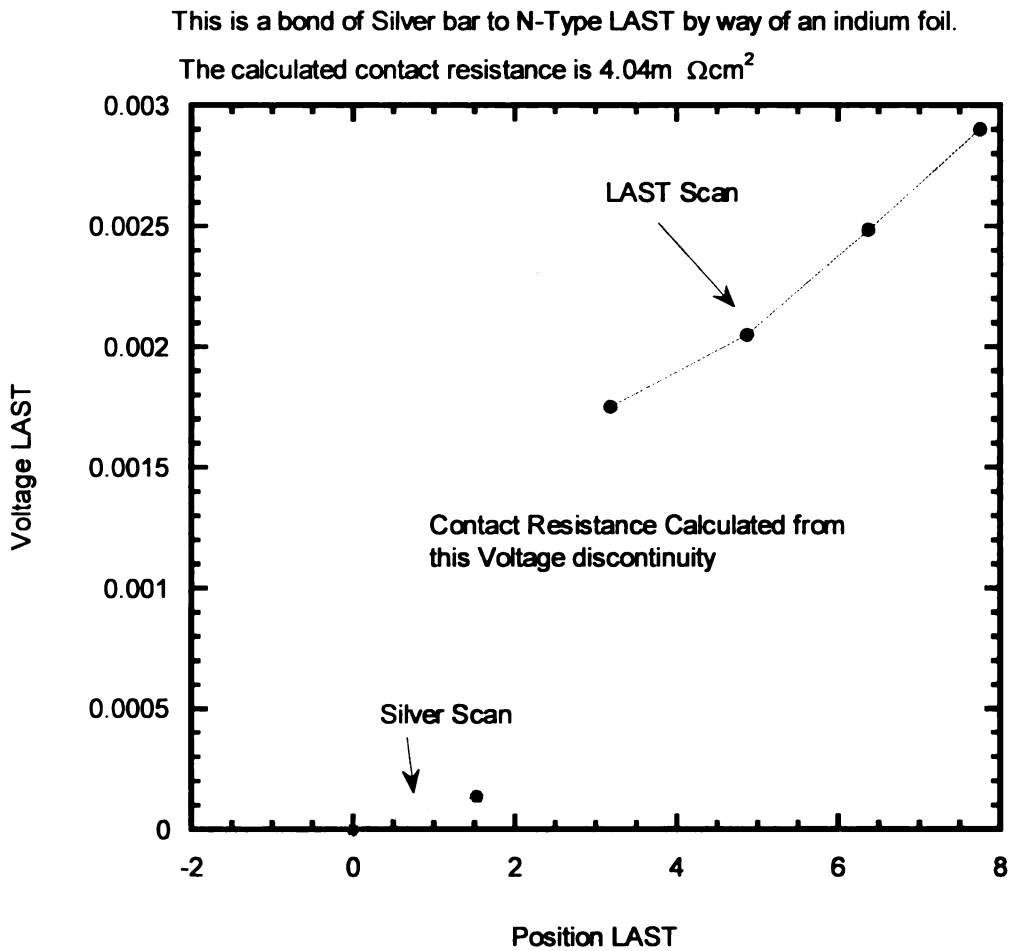

Figure 51: Silver to N-type LAST voltage profile scan across contact

This contact scan shows a resistance of around 4mΩcm^2. This is much too high for making an efficient device.

8.4 Antimony to LASTT Contact Scans

A bond was done with antimony directly to LAST in order to see what the contact voltage profile would look like.

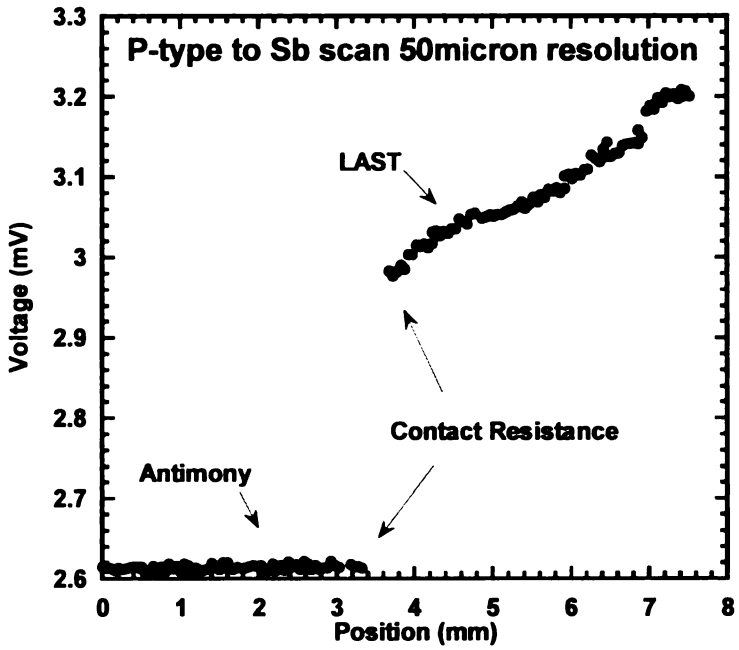

Figure 52: Antimony to LAST contact Scan

The data shows a large voltage discontinuity at the interface between the LAST and the antimony and measures a contact resistivity of $525\mu\Omega cm^2$. This is still much too high for good module fabrication. The contact resistances previous results because the temperature and time used during the fabrication processes are different. A lower temperature was used during this run to help sample integrity and reduce outgassing.

Figure 53 shows the results of contact resistance measurements for a LAST-Sb-LAST structure bonded at 590°C at 300Torr for 10 minutes. Previous antimony bonds were done under in a sealed quartz tube at temperatures around 700°C.

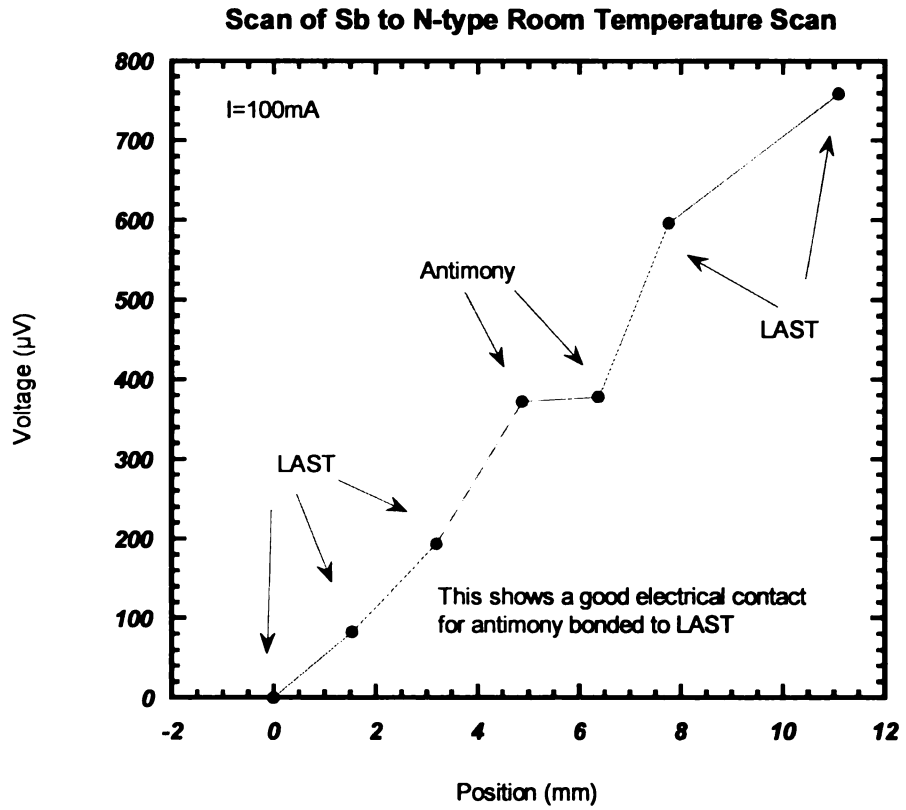

Figure 53: LAST-Antimony-LAST Contact Scan

The voltage drop at each Sb-LAST junction is less than 200μV for contact resistance less than 2mΩ. This sample had a cross section of 3.51mm x 5.00mm giving a contact resistivity of less than 461μΩ·cm^2. This value is similar to the previous Sb-LAST contact, and is too high for device fabrication. The fabrication process used early must be used to achieve low enough contact resistances to build an efficient device.

8.5 BiSb Alloy Contact Scan

An alloy of bismuth – antimony has been found to make a good mechanical contacts to LAST. The phase diagram for Bi-Sb is shown in Figure

53, where it can be seen that for a solder melting point of less than 500°C, the weight percent concentration of bismuth must be greater than 60%.

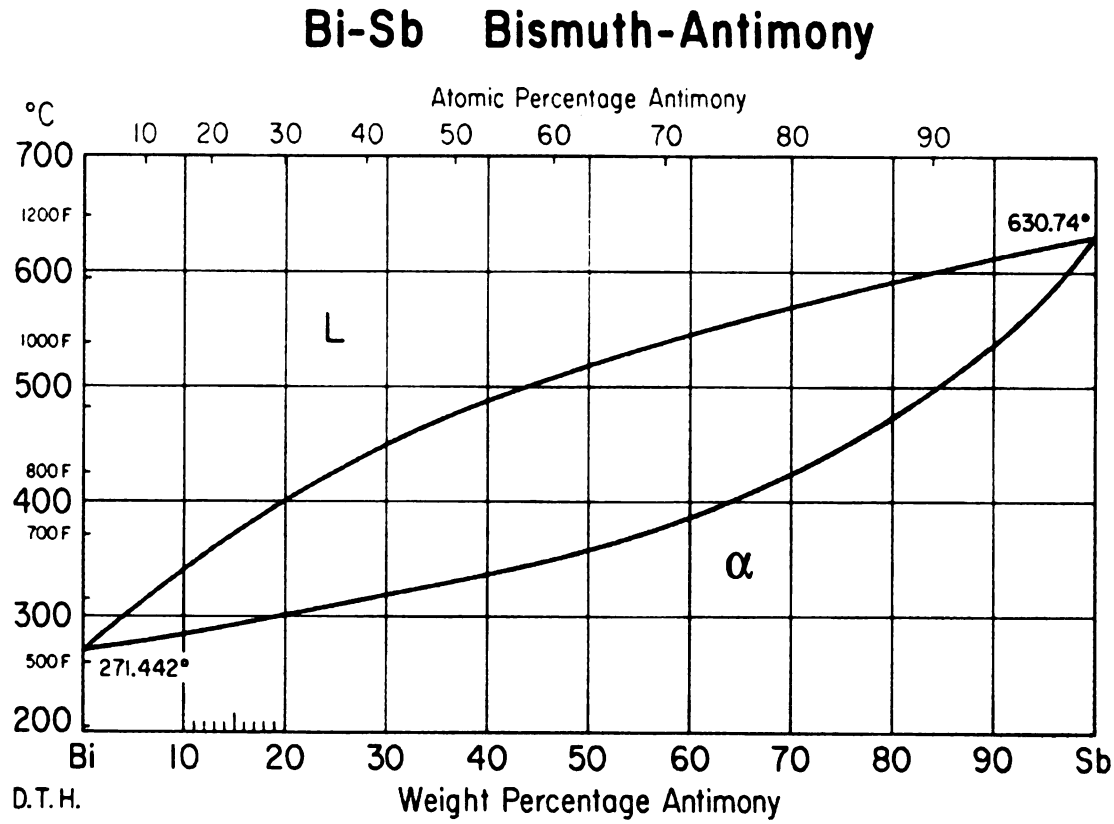

Figure 54: Phase diagram for bismuth - antimony alloy [13].

The bond was fabricated at a temperature of 500°C for 10minutes at 300Torr. After the run was completed, there were no signs of outgassing of the LAST.

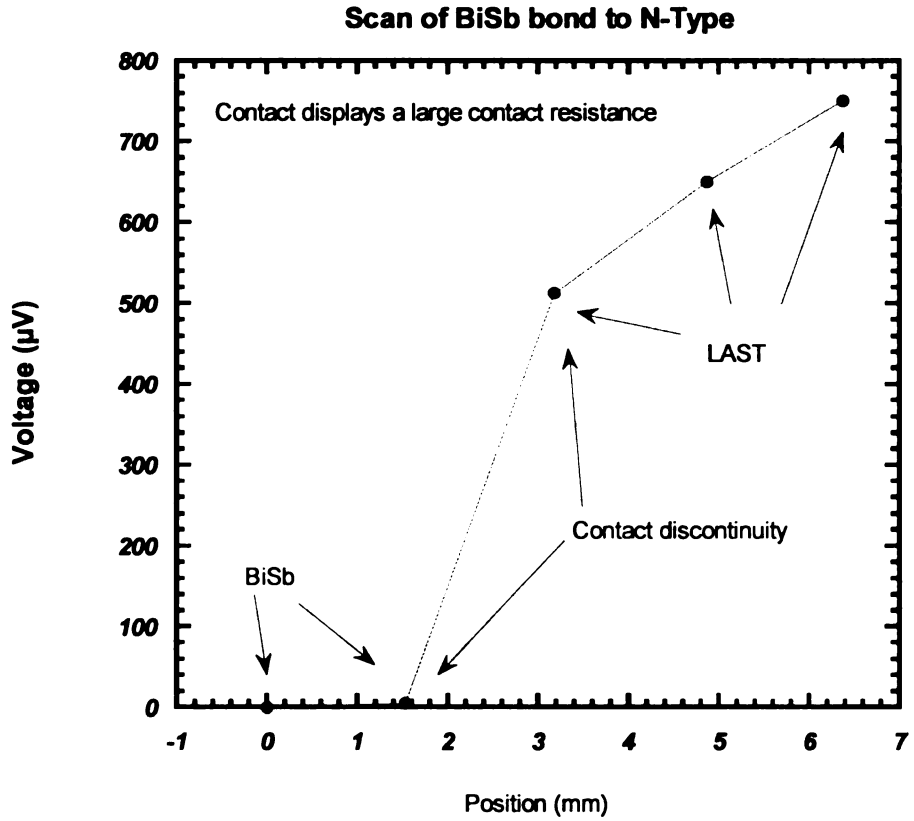

Figure 55: BiSb alloy to LAST contact scan

The contact resistance calculated for the BiSb bond is 1.152mΩcm^2. Although the bond strength is strong mechanically, this material has to be abandoned due to the very high contact resistance.

8.6 Gold Silver Alloy Bond

A 50-50 weight percent alloy of gold - silver was made and bonded to LAST and LASTT materials as shown in Figure 56. The bond was formed at 650°C for 10 minutes with no pressure applied to the junction during bonding.

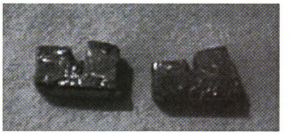

Figure 56: Gold silver alloy bonds

The alloy did bond to the LAST and LASTT materials, however the alloy also catalyzed the melting of the samples. Low melting point materials such as indium have been shown to form low resistance contacts to PbTe by forming a new compound during the bonding process (InTe in this example) which is then stable to much higher temperatures [14]. Large quantities of the low melting point material would consume too much of the sample in forming the new compound, therefore such materials are best investigated as thin films or thin foils at the interface between the sample and a high temperature metal interconnect.

Chapter 9 New Diffusion Bonding Techniques and Stainless Steel Bonds

9.1 Higher Pressure During Bonding

To investigate the pressure dependence during bonding, a stainless steel clamping structure shown in Figure 56 was constructed. A 500μm thick tungsten foil was placed on an n-type LAST sample and clamped between the stainless steel plates as shown in Figure 57.

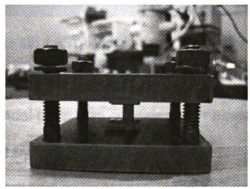

Figure 57: Stainless steel bonding block

The bond to the tungsten was attempted at 755°C for eight hours. The argon gas pressure in the chamber remained near atmospheric pressure during the 8 hours. It was found that the tungsten did not bond to the LAST, however the LAST material did strongly bond to the stainless steel plate as shown in Figure 59.

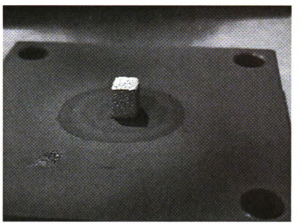

Figure 58: LAST bonded directly to stainless steel

Although the stainless steel plate was considerably heavier than the LAST sample, it could be lifted by the LAST sample without breaking it off the stainless steel. Based on this result further investigations of bonding stainless steel to the LAST and LASTT materials was initiated. To apply some pressure on the contacts during bonding, a new sample holder was designed.

9.2 Diffusion Boat Improvements

Prior to beginning more investigations into bonding stainless steel, a way of adding weight was needed to aid in the bonding process. Glass shop cut quartz pieces that could individually sit on top of each unicouple to add weight to the bonding process.

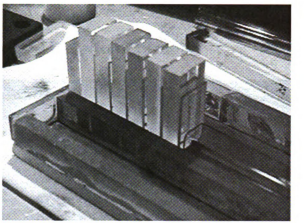

Figure 59: Added quartz pieces for weights during diffusion bonding

9.3 Initial Stainless Steel Diffusion Attempts

Figure 60: First diffusion bon of LAST and LASTT to stainless steel 725°C 330Torr for the run

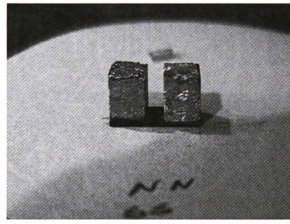

Figure 61: N-type bond at 725°C

The p-type turned black and showed signs of pitting.

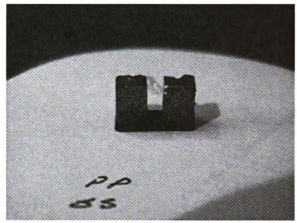

Figure 62: P-type bond at 725°C

The conclusion was to keep attempts at lowering the bonding temperature and increasing pressure. Initial contact measurements gave a contact resistivity of 140$\mu\Omega cm^2$. Later bonds done at lower temperatures (near 700°C) showed very low contact resistivities to p-type legs as shown in Figure 63.

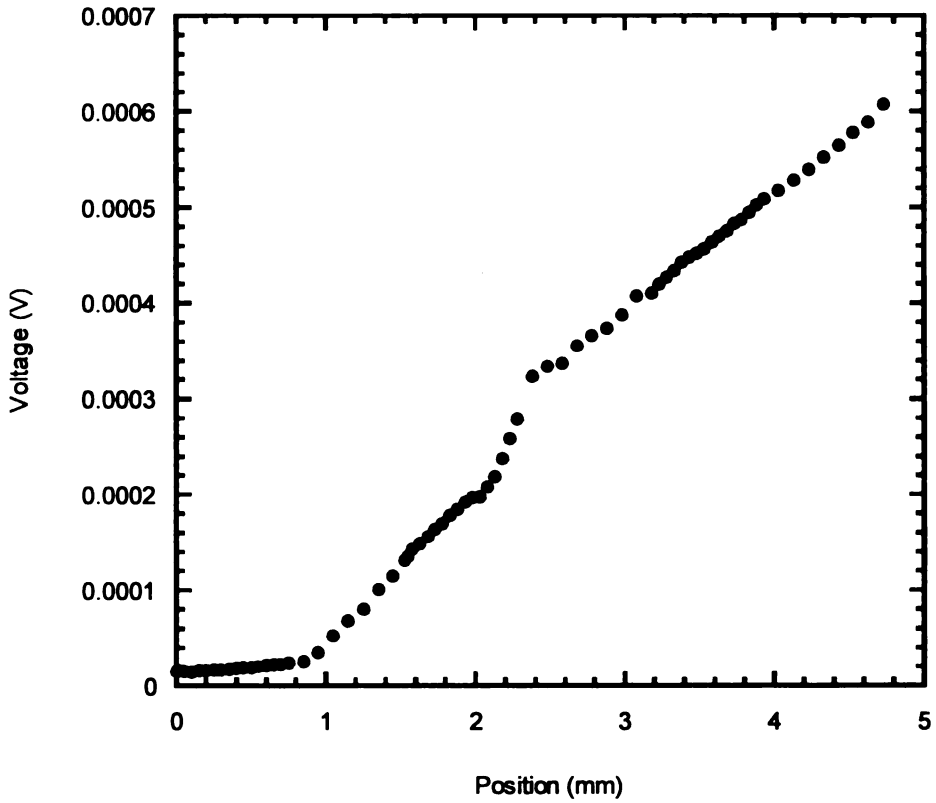

Figure 63: P-type to stainless steel contact scan

The bond shown in Figure 63 was formed using additional weight during the bonding process.

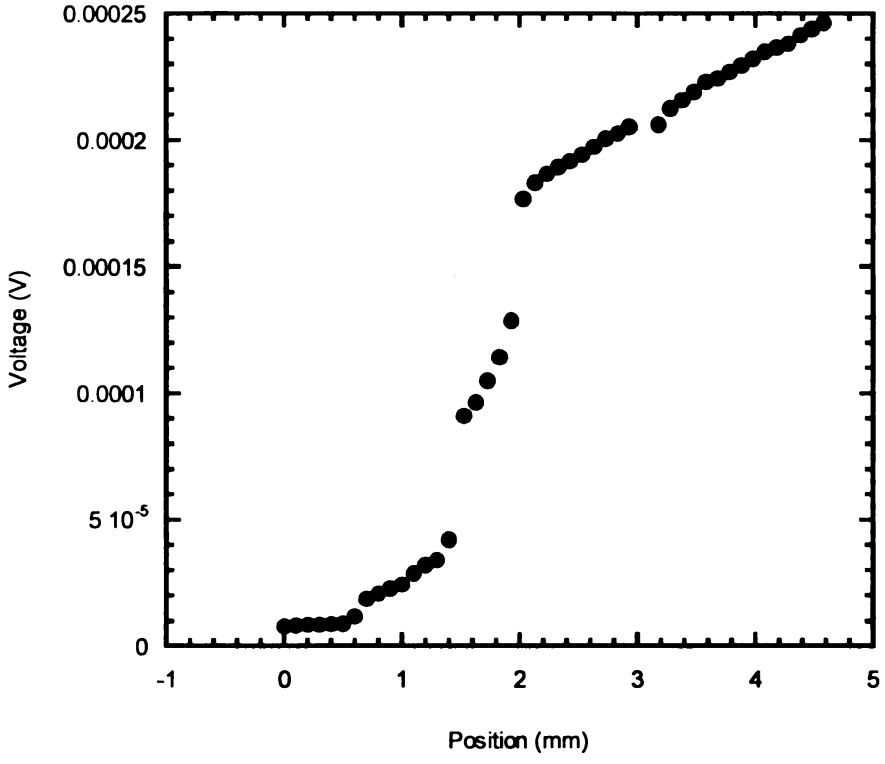

Figure 64: N-type to stainless steel contact scan

Bonding stainless steel to the n-type (LAST) samples also showed a relatively low contact resistivity (Figure 65). To further investigate the influence of pressure during the bonding process, a new unicouple boat was designed.

9.4 New Unicouple Boat

A new unicouple boat was design to give each individual unicouple an amount of pressure through adjustments of a set screw in order to make a good interface bond. A side profile of this new boat is shown in Figure 65.

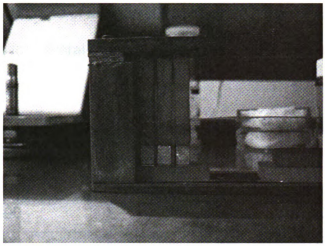

Figure 65: New unicouple boat

The first bonds made from the boat showed lower contact resistances of 50-100$\mu\Omega cm^2$ and increased mechanical strength.

9.5 New Reducing Gas

To help remove oxides at the interface, a (5% H_2) / (95% Ar_2) gas mixture was used in place of the pure argon gas.

9.6 Stainless Steel Bond Investigations

The following is a table listing the bonding temperature and times used to bond LAST and LASTT to stainless steel. Chromium was also investigated for bonding to p-type LASTT for comparison. All contact resistance values were measured using the room temperature scanning probe also developed as part of

this work. Photos of some of the bonds investigated can be found in Appendix A, and voltage scans for several of the experiments listed in Table 4 can be found in Appendix B.

Table 5: Diffusion bonds and corresponding contact resistances

Bridge Material	Bonding Temp °C	Bonding Time Hrs.	Pressure Torr	Contact Reisistance $\mu\Omega cm^2$
P/SS	690	1	92	274
P/SS	690	1	92	195
N/SS	690	1	92	131
N/SS	690	1	92	75
N-SS	690	2	80.3	250
P-SS	690	2	80.3	129
P-CHR	690	0.5	138	112
N-CHR	690	0.5	138	Cracked
N-SS Hand Tighten	690	3	168	~5
N-SS new boat (NB)	690	0.75	300	Cracked
P-SS NB	690	0.75	300	70
P-SS NB		1	297	~5
P-SS NB		1	297	90

Chapter 10 Summary and Future Work

10.1 Summary

This thesis focuses on the investigation of electrical contacts to new thermoelectric materials for the development of power generation devices. As part of this effort systems and methods for measuring contact resistances have been established, including a transmission line technique and a scanning probe technique. The scanning probe technique is useful for configurations which are amiable to device fabrication, and the transmission line technique gives increased accuracy on the measurement. Many different alloys have been deposited and measured for contact resistance (Table 2). A diffusion bonding system has been designed and assembled for investigating high temperature contacts through diffusion bonding. This system has been designed to accommodate several modules during the bonding process and/or individual unicouples. Utilizing this system various metals and alloys have been investigated for forming these high temperature bonds and tested with the measurement systems developed (Table 3). Several promising contacts have been identified with contact resistivities less than $60\mu\Omega\cdot cm^2$.

10.2 Future Work

Diffusion bonding studies have indicated the formation of tellurides during bonding, therefore future work will include depositing excess tellurium at the contact interface to assist in the bonding process and help prevent tellurium diffusion out of the semiconductor samples. The investigation of InTe and SnTe

contacts will also be further investigated. Pressurization of the diffusion bonding system during bonding has significantly helped to reduce outgassing from the samples, and high temperature sealant coatings will be investigated for encapsulation of the samples to further prevent them from outgassing.

APPENDIX A

Diffusion Bonds and Results

Figure A 1: $ZnCl_2$ pre-etch + Sb powder, no bond (out-gassing)

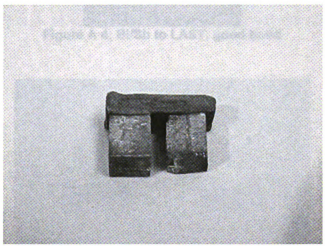

Figure A 2: Sb, good bonds (no out-gassing)

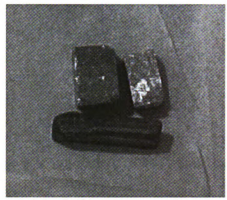

Figure A 3: Bi/Sb (55/45) on Ni, no bonds

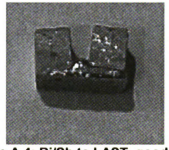

Figure A 4: Bi/Sb to LAST, good bond

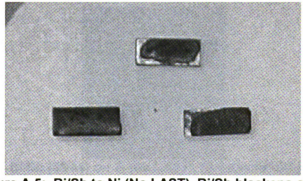

Figure A 5: Bi/Sb to Ni (No LAST), Bi/Sb blackens on Ni

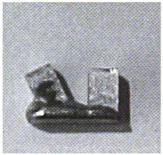

Figure A 6: Sb only to LASTT, Good Bonds

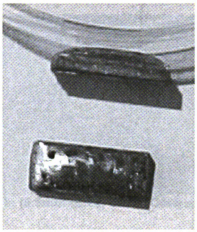

Figure A 7: Sb on Ni (No LAST), Not Bad- A little blackening

Figure A 8: Bi/Sb (55/45) on Ti (no LAST), Good bond between metals

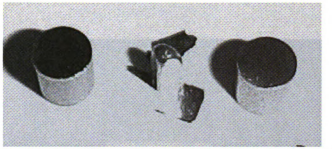

Figure A 9: Bi/Sb (55/45) on W (no LAST), no bond between metals

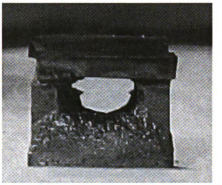

Figure A 10: In (0.5mm thick) on Ni, Consumed samples

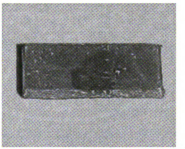

Figure A 11: In on Ni (No LAST) Good bond between metals

Figure A 12: In on Nickel to LAST (prealloyed), Good Bond

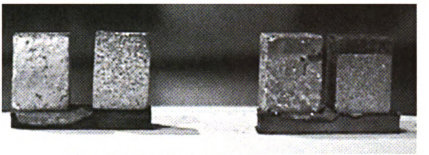

Figure A 13: In 1mm thick on Ni, Good Bond

Figure A 14: Stainless steel to LAST, good Bond

APPENDIX B

Contact Resistance Scans

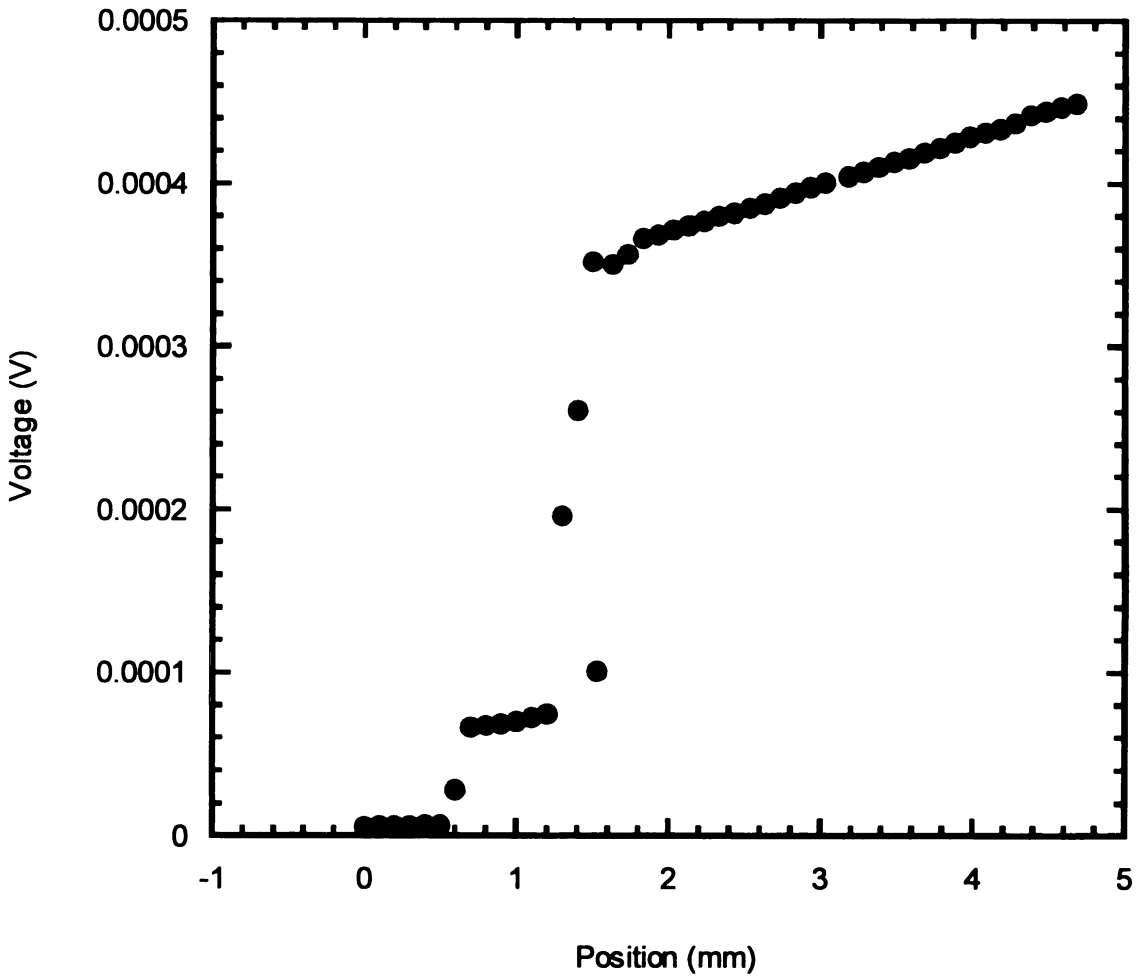

Figure B 1: N-type to Stainless Steel, 690°C 1 Hour, 138μΩcm^2

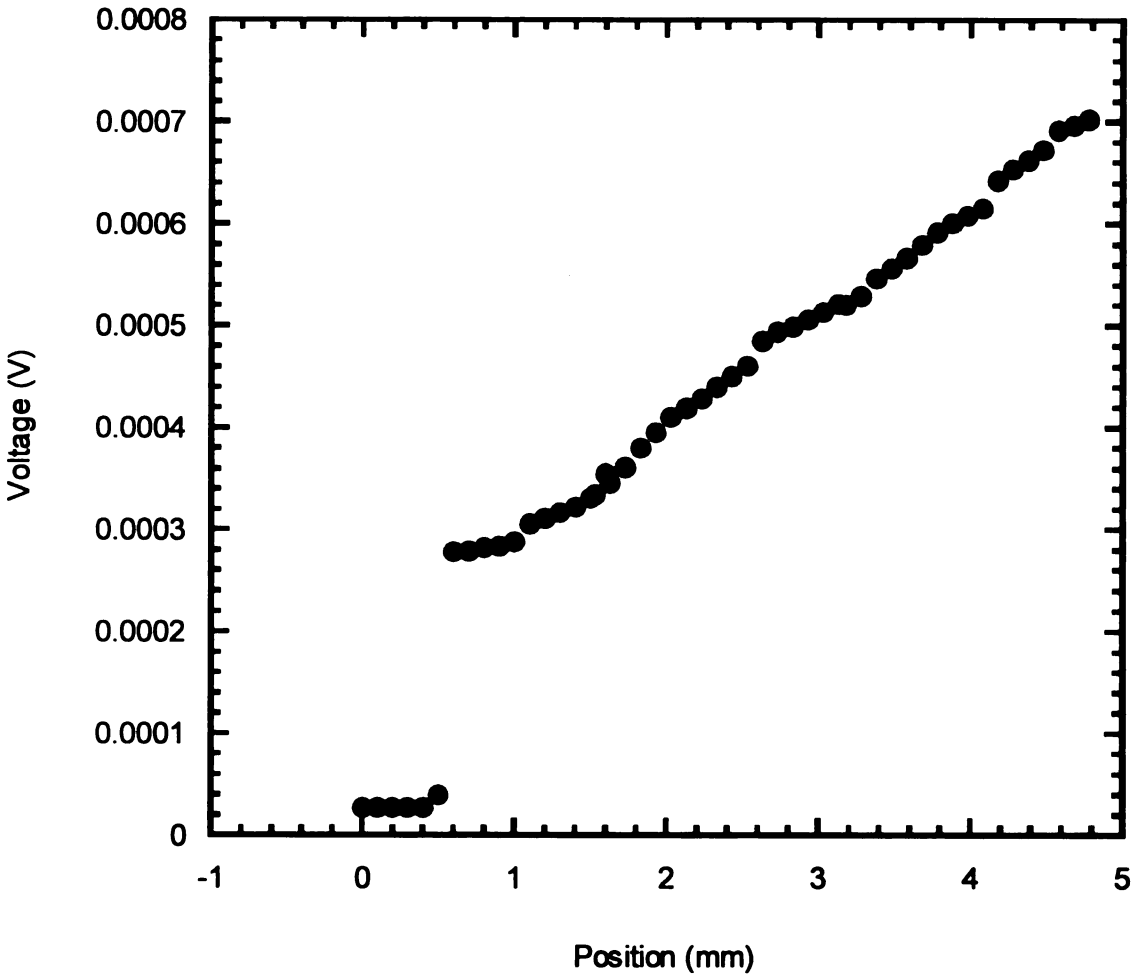

Figure B 2: P-type to Stainless Steel, 690°C 1 Hour, 195μΩcm²

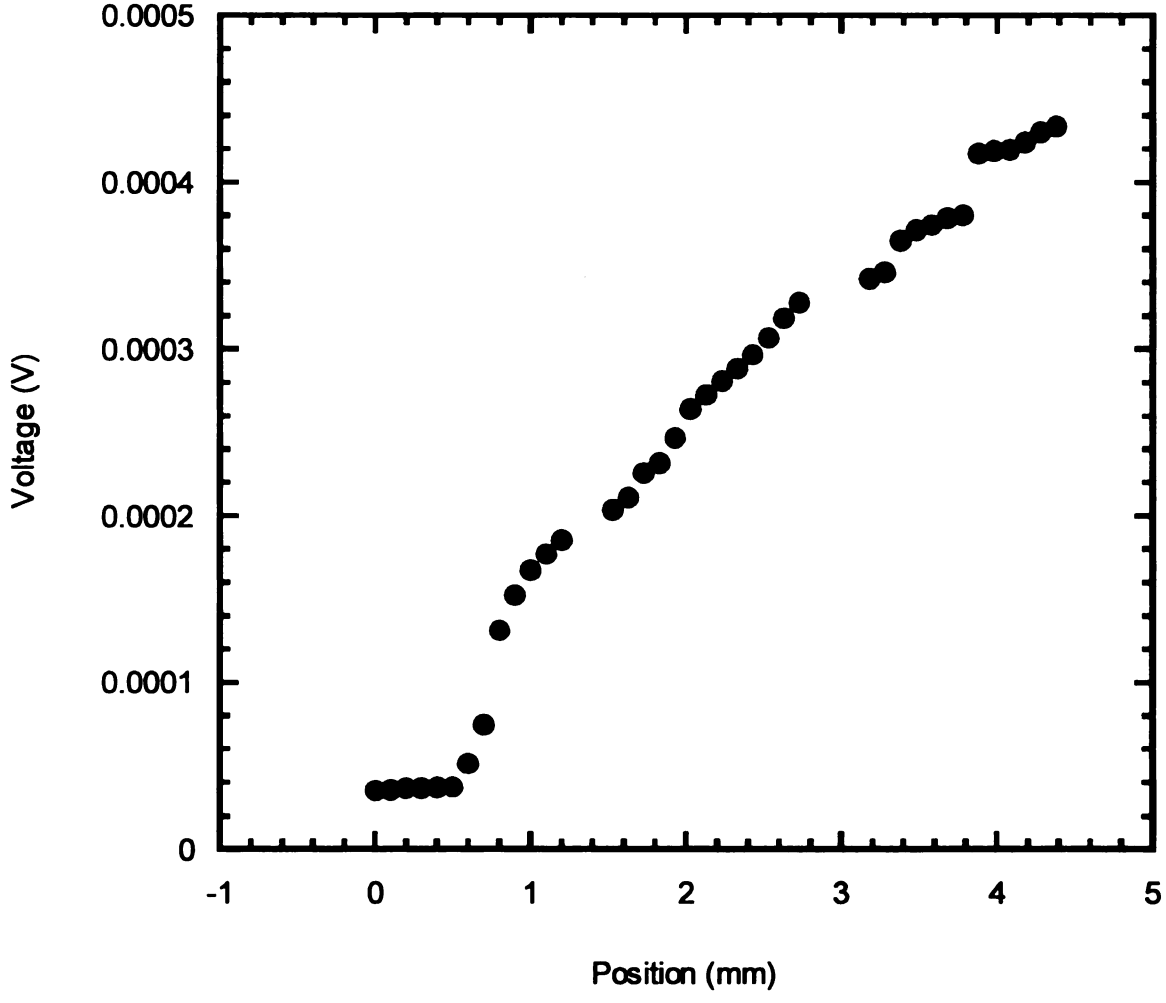

Figure B 3: P-type to Stainless Steel, 630°C 4 Hours, ~5μΩcm²

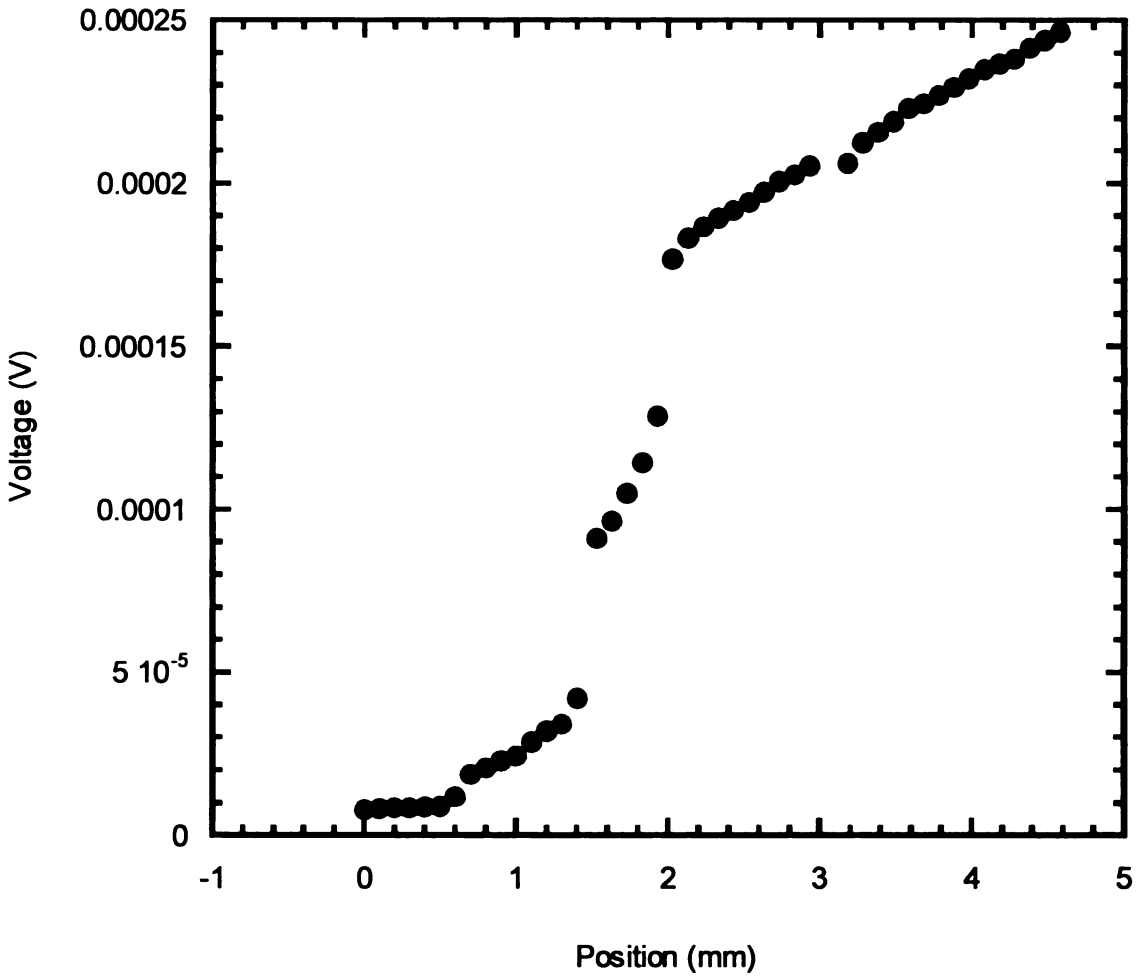

Figure B 4: N-type to Stainless Steel, 700°C 4 Hours, ~5μΩcm^2

BIBLIOGRAPHY

[1] H.J. Goldsmid, "Thermoelectric Refrigeration." Plenum, New York, NY, 1964.

[2] H.J. Goldsmid, "CRC Handbook of Thermoelectrics," ed. D.M. Rowe (1995)

[3] Sim Loo, "Transport Characterization of New High Temperature Quaternary Thermoelectric Materials And Devices", Ph.D. thesis, Michigan State University, 2003.

[4] M. G. Kanatzidis, "The Role of Solid-State Chemistry in the Discovery of New Thermoelectric Materials," in *Solid State Physics*, ed. H. Ehrenreich, F. Spaepen, vol. 69, pp 51-100, Academic Press, New York, 2001.

[5] Kuei Fang Hsu et al., "*Cubic $AgPb_mSbTe_{2+m}$ Bulk Thermoelectric Materials with High Figure of Merit,*" Vol. 303, Science, www.sciencemag.org

[6] A. F. Ioffe, *Semiconductor Thermoelements and Thermoelectric Cooling*, Infosearch Limited, London, 1957.

[7] L. D. Hicks, M. S. Dresselhaus, "Effect of Quantum-Well Structures on the Thermoelectric Figure of Merit," *Physical Review B*, Vol. 47, No. 19, pp. 12 727-12 731, 1993.

[8] T. C. Harman, M. P. Walsh, B. E. LaForge, G. W. Turner, "Nanostructured Thermoelectric Materials," *Journal of Electronic Materials*, 34 (5), pp. L19-L22, 2005.

[9] M. H. Cobble, "Calculations of Generator Performance," *CRC Handbook of Thermoelectrics*, CRC Press, 1995.

[10] H.H. Berger, "Models for Contacts to Planar Devices," *Solid State Electronics,* 1972, Vol. 15, pp. 145-158.

[11] H. E. Bates, F. Wald and Martin Weinstein, "The Bonding of Lead Telluride with Non-Magnetic Electrodes," *IEEE/AIAA Thermoelectric Specialists Conference*, May 17-19, 1966.

[12] D.A. Porter and K.E. Easterling, "Phase Transformations in Metals and Alloys," 1993, Chapman and Hall.

[13] Massalski, T.B., "Binary alloy phase diagrams," Materials Park, Ohio : ASM International, c1990.

[14] Hittman.Associates, Inc. "Thermoelectric Bonding Study," Report Prepared for National Aeronautics and Space Administration, Goddard Space Flight Center, under Contract NAS5-3973, 1964.

MICHIGAN STATE UNIVERSITY LIBRARIES
3 1293 02845 2708